ALMA MATER STUDIORUM – UNIVERSITÀ DI BOLOGNA
CAMPUS DI CESENA

DIPARTIMENTO DI INGEGNERIA INDUSTRIALE (DIN)

Corso di Laurea Triennale in
INGEGNERIA BIOMEDICA

ANALYSIS OF BIOMECHANICAL IN VITRO TESTS ON THE HUMAN RIBS

Tesi di Laurea Triennale in
BIOMATERIALI E COMPORTAMENTO MECCANICO DEI MATERIALI (C.I.)

RELATORE:
Chiar.mo Prof. Luca Cristofolini

PRESENTATA DA:
FRANCESCO MARCONI

CORRELATORE:
Dott. Ing. Marco Palanca

SESSIONE II
ANNO ACCADEMICO 2018/2019

Alla mia Famiglia…

Summary

Abstract

In questa Tesi viene descritto il processo di elaborazione dei dati ottenuti su costole umane sottoposte ad un carico flessionale e motiva i risultati ottenuti, con l'obiettivo di ottenere una loro caratterizzazione meccanica. Svolgendo funzioni di protezione vitali per l'essere umano, lo studio dal punto di vista ingegneristico di tali elementi anatomici assume una certa importanza in quanto permette la determinazione delle condizioni limite entro le quali la costola umana garantisce le sue complete funzionalità. Questo elaborato fa parte di un progetto più ampio eseguito in collaborazione con l'Università di Ulm.

Non è stato trovato nella letteratura scientifica uno studio sul comportamento meccanico di tali strutture anatomiche, per cui i risultati riportati in questo lavoro potrebbero costituire un parziale punto di partenza per ricerche in questo settore poiché si basano sullo studio di 91 provini che garantiscono una certa affidabilità dal punto di vista statistico.

Prima di entrare nella trattazione dell'argomento, è stata descritta l'anatomia delle costole e sono stati presentati i principi alla base di concetti teorici e della strumentazione usata per comprendere appieno lo studio dal punto di vista anatomico, ingegneristico e statistico.

L'elaborazione dei dati può essere suddivisa in tre fasi, che permettono uno studio dal punto di vista meccanico delle costole dall'aspetto globale fino a quello specifico. In primis sono stati calcolati i valori dei carichi di rottura, dei moduli elastici e delle energie assorbite per tutti i provini testati dalla macchina di prova; successivamente i valori ottenuti sono stati organizzati per livello costale, in modo da poter osservare possibili relazioni tra posizione nella gabbia toracica e caratteristiche meccaniche. Per un'analisi più specifica è stata eseguita una correlazione spaziale per tutte le costole di cui sopra usando un software per la DIC che permettesse di valutare le deformazioni dovute al carico applicato. Tali valori sono stati utilizzati con l'intento di comprendere le cause dei tipi di fratture verificatesi nei diversi provini. Dopodiché i valori di carico e modulo elastico sono stati confrontati con i dati forniti dalle micro-CT eseguite su ogni costola in modo da trovare una relazione tra il comportamento meccanico e la mineralizzazione della costola.

Dall'analisi globale si è potuto osservare un particolare andamento dei valori di carico di rottura e modulo elastico al variare delle posizioni delle costole nella gabbia toracica mentre i valori delle deformazioni calcolati dalle correlazioni non hanno prodotto alcun risultato notevole, se non indicare la presenza di un momento torcente agente sui provini oltre a

quello flessorio impostato. I dati delle micro-CT invece confermano quanto detto legando le caratteristiche meccaniche ad una certa quantità di tessuto osseo. Inoltre i valori del rapporto $\frac{Bone\ Volume}{Tissue\ Volume}$ indicano una possibile relazione sia con i carichi di rottura che con i moduli elastici.

Abstract

In this Thesis the process used to obtain mechanical information about human ribs subjected to a flexion load is described. This work belongs to an important project carry out by the University of Bologna and the University of Ulm.

In the scientific literature there are not studies about the ribs' mechanical behaviour; thus, the results obtained in this work could be used for next studies because they are based on the study of 91 human specimens which guarantee a statistical reliability.

Initially the ribs'anatomy and the instrumentation is described, and the basic principle of Biomechanics and Statistical theories are provided in order to better explain the experimental tests and results.

The data elaboration is divided in three steps in order to have a complete description of ribs mechanical behaviour. First break loads, stiffnesses and absorbed energies are calculated for all the specimens properly tested. Then these values are organised in order to observe the differences between different rib levels. Using DIC method it is possible to study the strains developed during the tests on the specimens. The values obtained are studied to understand the break reasons. After that the mineralization levels provided by the micro-CT scans for each rib are studied in order to find a relationship with the rib failures.

From the first step it is possible to observe that break load and stiffness values are linked to rib position in the ribcage. Conversely the strain study does not provide any remarkable results apart from showing the presence of a torsion during the tests.

The micro-CT data confirm that mechanical characteristics are linked to bone tissue quantity. In addition, $\frac{Bone\ Volume}{Tissue\ Volume}$ values could be linked to break load and stiffness values.

Chapter 1 – Introduction

1.1 A general view

The human body anatomical structures are due to a long evolutionary path which led to an optimization of various organs and apparatuses for certain purposes. The Biomechanics, through engineering knowledges, explains how the human body adapts due to a continuous interaction with the surrounding environment. The engineering study of human body requires lot of work due to the variability of numerous factors like genetics, sex, age, health conditions. Apart from their availability, human specimens acquisition has to be approved by ethical agencies. However, there are several studies made on animal specimens similar to the human ones which gave important results.

Biomechanics studies also the musculoskeletal system to obtain information about its mechanical properties; the results are useful to understand how the bones re-modelling works, why there are different shape between bones, which material could be used in prosthesis, how design them and give solutions to other issues. For instance, one of the best prosthesis nowadays is the hip one because were made several studies on the joint and the materials used.

Despite their importance in protecting the thoracic cavity, in the scientific literature there aren't lot of studies about the ribs' mechanical behaviour [1–4]. Apart from the complexities linked to studying human specimens, this lack of knowledge is probably due to the ribs' shape which causes less precise measurements.

This Thesis faces up the human ribs' behaviour from the fourth to the eighth one studying 91 specimens. Before explaining the work, first a general view about the anatomy, engineering knowledges and calculus flow is provided. The work is divided in three parts:

- Global analysis: it provides a general view of the entire ribs' mechanical properties;
- Local analysis: the local strains are measured thanks to the DIC method.
- Micro-CT comparison: the data from micro-CT scans are acquired and correlated to ribs mechanical properties.

Subsequently the results are discussed.

1.2 Ribs' anatomy

The bones are divided into three groups:

- Long bones: the length is bigger than width and thickness.
- Flat bones: the length and the width are bigger than thickness.
- Short bones: the three dimensions are equal each other.

The ribs, despite their size, belong to the flat bones for their structures. Indeed, they have trabecular tissue inside the cortical bone layer. As the other flat bones, the ribs have a good resistance to impacts and protect the organ inside the ribcage.

The following description is based on the anatomy book "Gray's Anatomy".

The ribcage is constituted by twelve thoracic vertebrae, twelve pairs of ribs, the costal cartilages and the sternum. We'll focus only on ribs: they are connected with vertebrae and, except for the last two ribs, with the sternum. The ribs are divided in two groups[1]:

- The "true ribs" connected directly with the sternum through the costal cartilages.
- The "false ribs" separated in two types: from the eighth to the tenth, their costal cartilages are connected each other and then they fix on the costal cartilages of the seventh rib. The eleventh and the twelfth, called the "floating ribs" do not attach to the sternum although they have cartilages in the end.
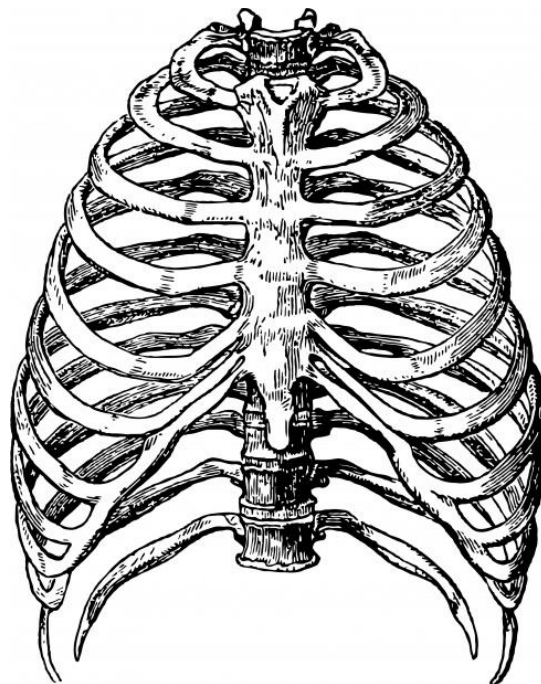

Figure 1.2-1: The ribcage.

Each rib is composed by the following anatomical part[5]:

- Head: it is the posterior ending and it has two articular facets that articulate with two vertebrae.
- Neck: it has less thickness and connects the head with the body. Here it is recognizable a bone crest.
- Tubercle: it is positioned between the neck and the body and it has a facet that articulates with the corresponding vertebra.
- Shaft: the external convex surface and the internal concave one are separated by a top margin and a lower one in which can be recognized the costal groove where costal nerves and vessels pass.
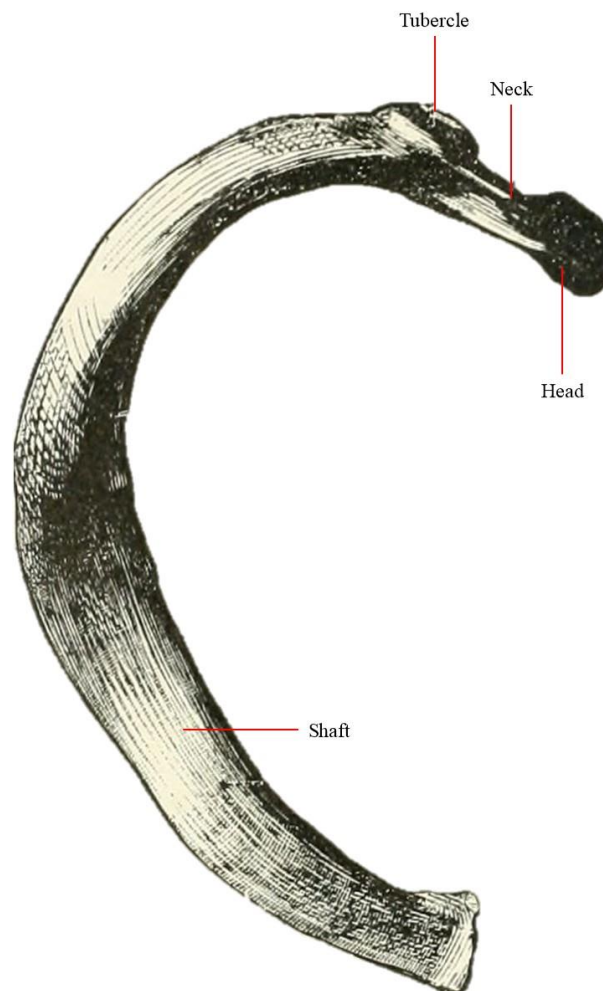

Figure 1.2-2: Top rib view.

Not all the ribs follow the structure below described[5]:

- The first one has a superior and an inferior surface with a medial and a lateral margin, with a swelled tubercle. Despite the other ribs, the body hasn't the costal groove.
- The second one is similar to the first but longer.
- The eleventh and twelfth are quite short and they have the head with only an articular facet which connect them with the eleventh and the twelfth vertebrae respectively.
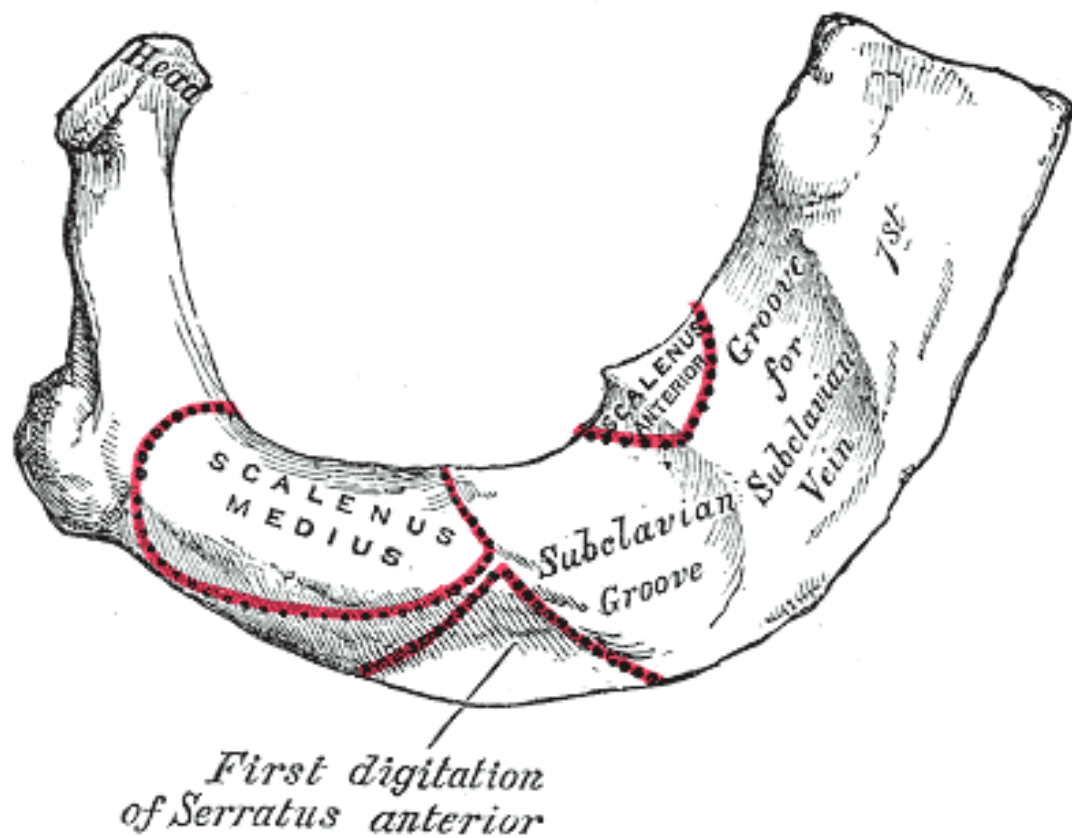

Figure 1.2-3: First rib from top view.

According to their anatomy the ribs protect the contents of the thoracic cavity and mediastinum and permit a proper breathing thanks to the muscles involved in inhalation and expiration.

1.3 Brief biomechanical notions

To understand the material mechanical behaviour, it is necessary considering the concept of deformation and tension beside load and displacement[6].
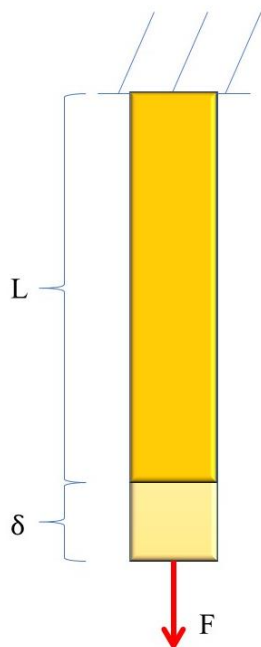
Let's consider a beam subjected to a load (P) as in the Figure 1.3-1. In these conditions, the beam will increase its length. The strain (ε) is a dimensionless value due to the ratio between the length variation and the initial length. The stress (σ) is the ratio between the force and the section in which is applied; it is usually measured in megaPascal (MPa= [N/mm^2]). If σ>0, the material is subjected to traction, whereas a σ<0 indicates a compression.

$$\sigma = \frac{F}{A}$$

$$\varepsilon = \frac{\delta}{L}$$

Figure 1.3-1: Beam subjected to load.

The two values are useful to describe how a material reacts to certain loads if we combined them in a diagram stress-strain. Usually in Biomechanics the ribs are a "fragile" material, as the other bones. This means that there is a proportional dependence between strains and stress; in other words, a fragile material has an "elastic" behaviour. This mechanical property allows to resist to increasing tension until the failure point where the material breaks.

Another concept is the "Young modulus" (E) defined as the ratio between stress and strain at the break point. It represents the proportional coefficient between stress and strain. It is measured in MPa. Due to their nature, the fragile materials failure is caused by the σ.

$$E = \frac{\sigma}{\varepsilon}$$

In order to break a material, it is necessary to apply a certain quantity of energy. The material capacity to absorb energy is described by "u" (MPa or j/cm^3) which is the area

underlying the curve stress-strain. It represents the evolved energy during the load application until the break point.

$$u = \sigma\, \varepsilon$$

Now it is possible to deepen the stress concept. If we consider the Figure 1.3-2, the applied force is directed along the x axis. Therefore it is possible to calculate σ_x. As a consequence, it is possible to compute $\varepsilon_x > 0$.

$$\varepsilon = \frac{\sigma}{E}$$

Despite σ_y and σ_z are equal to 0, ε_y and ε_z are measurable and lower than 0. This is an ordinary property for all engineering material. Generally, stress along a direction determines both strain along the same direction and opposite strain along the others. This property is described through the "Poisson coefficient "(ν).
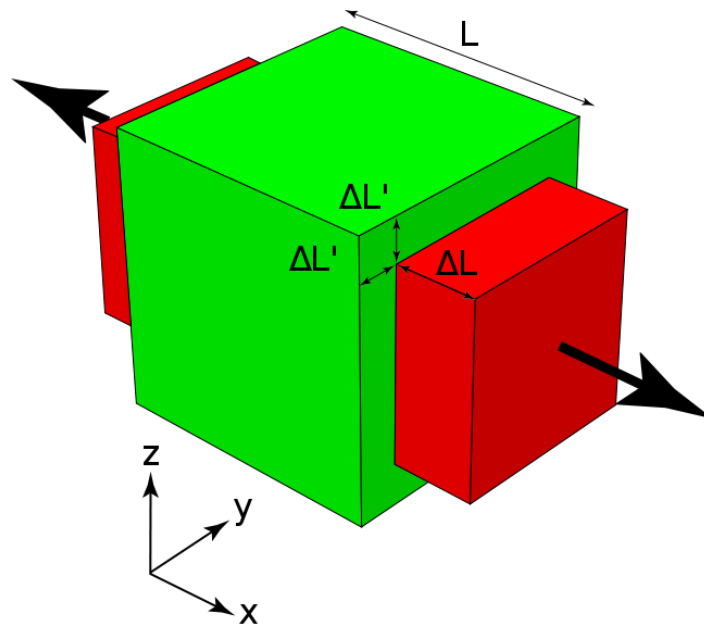

Figure 1.3-2: In this beam other ε occur with σ_x.

Another type of stress is the shear (τ), defined as the ratio between a force parallel to the material section (T) and the same section. The strain due to τ is called ɣ.

$$\tau = \frac{T}{A}$$

The σ and τ stresses are due to several reason. Their presence depends on both modulus and direction of the forces applied on the material. In this work it is useful to know that σ and τ stress measured on the ribs are due to flexion and torsion respectively. Flexion is due to a pair of opposite bending moment whereas torsion is due to a pair of opposite torques.
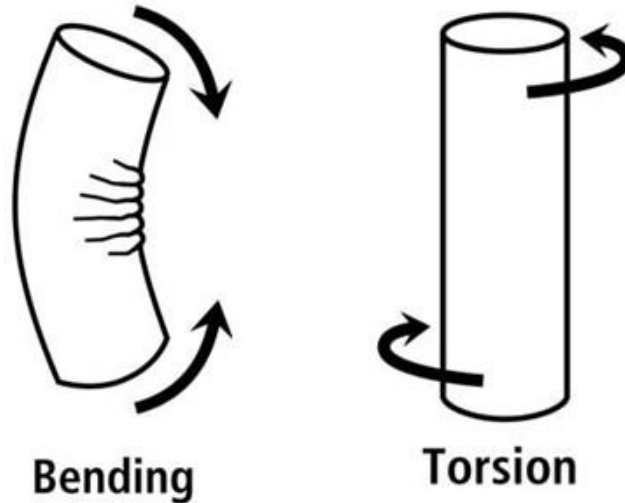

Bending   **Torsion**

Figure 1.3-3: Two examples of flexion and torsion.

In this way, according to a reference system, a material subjected to loads can be studied analysing the strains on a certain area. Therefore, a same deformation state can be described using more different references system. As a consequence, the stresses will change with the reference system used. In mechanics it is possible to describe a stress state with all the possible system references using the "Mohr's circle"[6].
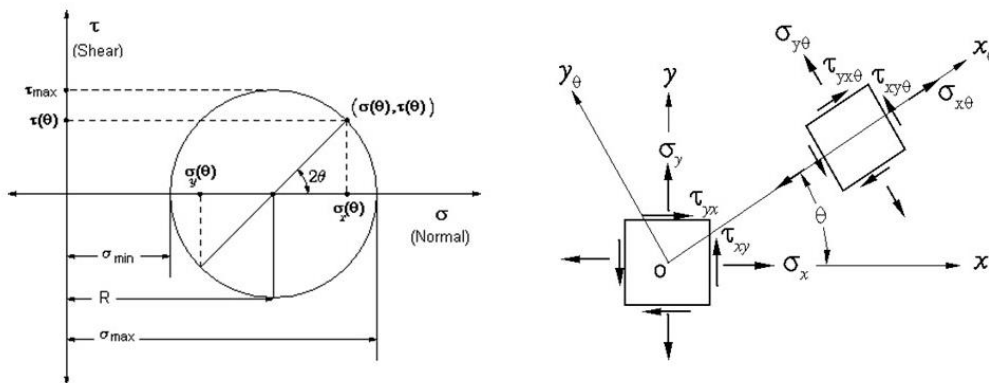

Figure 1.3-4: σ_x, σ_y, τ_{xy} represent the actual stress state. σ_{max} represents the maximum stress, σ_{min} the minimum one. ϑ is the angle between the actual reference system and the maximum stress one.

The Mohr's circle, for a certain stress state, allows to determine the maximum, the minimum stress and their reference systems through the angle computation.

This mechanic principles can be applied to the body structure; therefore, a general view about the bones' mechanical behaviour it is necessary. The bones properties are due to their structures and composition. Indeed the bones are made by lamellae which are mineralized connective tissue constituted by hydroxyapatite crystals in a collagen matrix[7].

Their arrangement defines:

- Osteons: the lamellae have a helix arrangement and they constitute the external bone layer called compact bone.
- Trabecular bone: it is composed by packs of bone lamellae. The trabeculae are arranged in order to transfer properly the stresses long the bone.
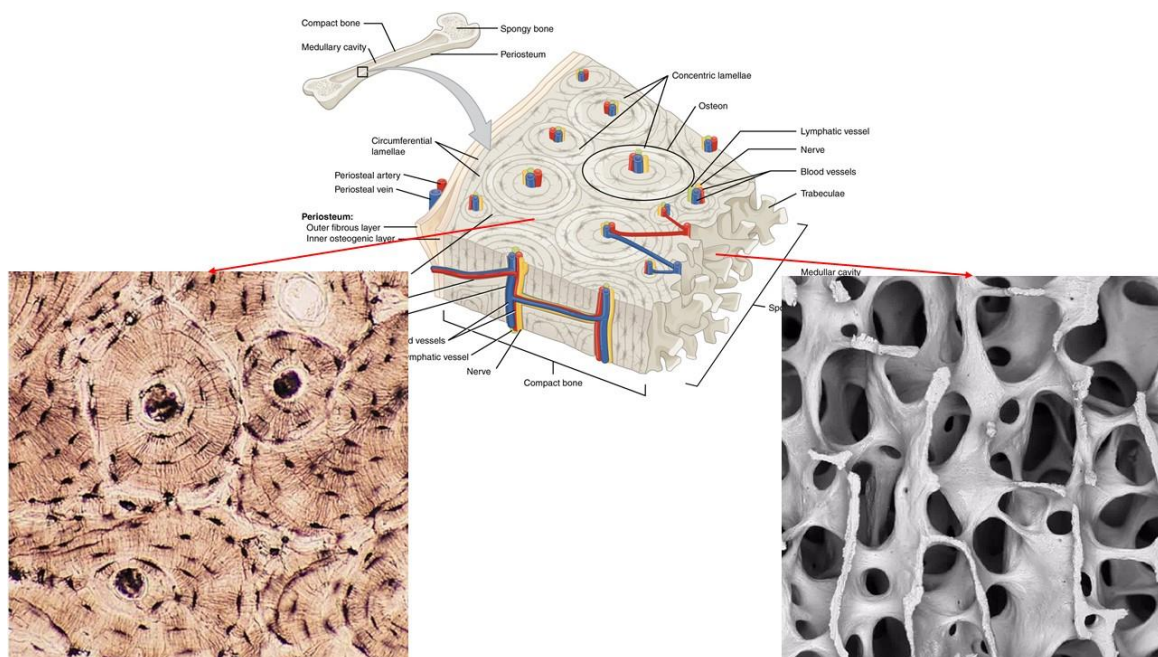

Figure 1.3-5: Cortical bone tissue and trabecular tissue in long bones.

This structure allows:

- Maximum strength;
- Minimum weight;
- Less metabolism;
- Less material waste;

The bones are optimized for their functions; they normally resist at their physiological loads. In case of accidents, other forces act on the bones which structure can't resist to them.

1.4 Computation process

In this Thesis all the ribs are described with a load-displacement graph measured by the load machine. This choice is due to the complications of using ribs' section (useful for stress calculus) for their irregular shape and variability. In addiction the displacements used for these graphs represent the machine movement during the test and not the specimen displacement. As a consequence, the values of stiffness and energy are measured respectively in N/mm and N. This limitation is explained in the "Limitation" subchapter The MATLAB (R2019a, The MathWorks, Natick, Massachusetts) "summary analysis" script is able to compute all the values described before using the load and the displacement measured by the machine.

To explain the calculus, it is useful to consider the following rib curve.
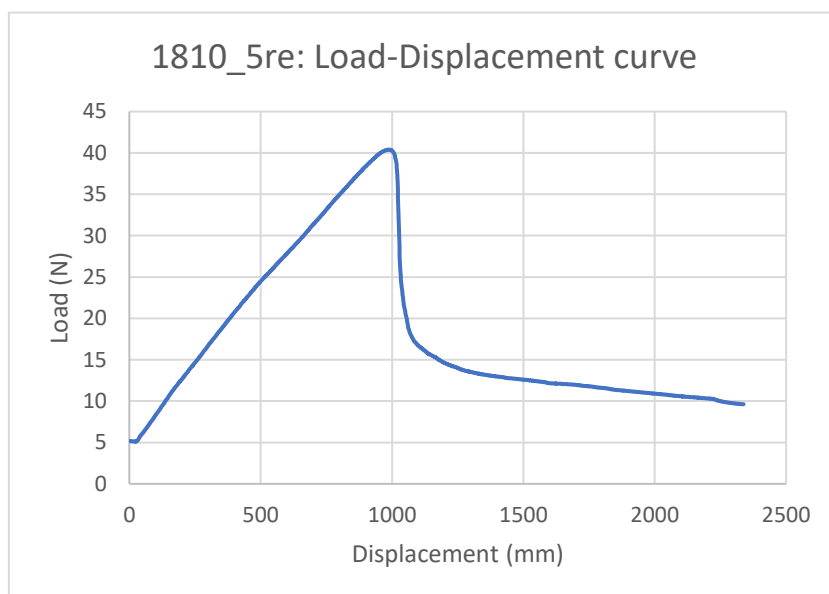

Figure 1.4-1: 1810_5re Load-displacement curve.

It is possible to observe that the load applied increase until a certain value; then there is a strong decrease. This means that the machine is forced to reach a certain shift; to do that an

increasing load is applied on the specimen. When the rib breaks, the machine applies less load to reach the shift imposed because the specimen does not offer resistance anymore.

The break load can be recognised because is the bigger load value reached. Then it is possible computing the stiffness through an interpolation of all load values until the break one. In this calculus, in order to obtain a correct Young modulus, are interpolated loads from the 10% to 90% of break load. This computation was made considering that the machine load exercises an offset of 5 N circa by default. The loads interpolation gives an accurate E value because the ratio between only the values of load and displacement measured at the point break could be affected by errors. The energy is calculated using a MATLAB function that computes the area underlying the curve load-displacement.

The calculations described above concern a global view of the ribs. In "Results" chapter there's a depth description about them.

A specific view is provided by the DIC method, as explained in the subchapter "A general view". Thanks to the DIC software, it is possible to observe the strains measured for each rib during the test phase. In particular the values of Eps1, Eps2 and ɣ are used. Eps1 and Eps2 represent the maximum and the minimum strain measured on the specimen; ɣ is the tangential deformation. This strain values can be used to create the Mohr's circle. In the previous subchapter, the Mohr's circle was described as a way to define a stress state: here the circle is used to describe a strain state using the same criteria. In the "Discussion and conclusion" chapter, the use of Mohr theory is discussed.

The Mohr's circle created allows to calculate the angle between the reference system and the maximum strain one. The following formula uses trigonometric rules.

$$\vartheta = \frac{\sin^{-1}\left(\dfrac{\gamma}{(\varepsilon_1 - \varepsilon_2)/2}\right)}{2}$$

The angle computation can be useful to understand the break reasons. The existence of a certain angle indicates that on the specimens were loads that determined both ε_x (and as a consequence ε_y) and shear.

The strain analysis is discussed in the "Discussion and conclusion" chapter.

At this point it is necessary an observation. The concepts described above are applicated on beams which are structure with length bigger than width and depth. As explained in "Anatomy" subchapter, the ribs are bones with a non-negligible curvature. Despite that, in this work the theory concepts explained are applicated on ribs.

1.5 The DIC method

The Image Correlation (DIC) is a contactless technique largely used among the tissue characterisation.

This method is based on images taken to the specimen during the experimental test thanks to one or more cameras. The first image taken on it, called "reference", shows the undeformed specimen. Then the load is applied, and the cameras continue to take images. In this way every frame records the specimen under an increasing load. As explained in "Brief biomechanical notion" subchapter, the load causes stress and strain. Comparing the reference with all the following frames, the DIC is able to calculate the strains thanks to a particular software. It recognises the specimen in every frame thanks to an algorithm which identifies every single region on its surface. Finally, it is able to compute the displacement for every single specimen region and, through derivation, the strains due to the increasing load. This is possible by choosing a reference frame for the undeformed state of the specimen and comparing to the others taken.

This method offers full field measurements of the specimens tested. Although the DIC is compromised by issues due to the optical approach.

1.5.1 The pattern

As just mentioned before, the software can identify the regions on the specimen surface thanks to a preliminary preparation. On the surface specimen is applied a random dot pattern: in this way every specimen's point has a unique dot distribution that make it recognisable from the others. The dot pattern strongly influences the DIC analysis because the strain computation is possible if there is a proper speckle pattern.

The preparation of the specimens requires less time rather than the conventional instruments like extensimeter. On the other hand, a proper pattern is mandatory to obtain

best results. As a consequence, the dots' size and roughtness, the pattern distribution, the black-white ratio and his contrast are the main parameters controlled for an optimal use of the DIC.

First a white background is created and the black dots are applied over it usually with an airbrush airgun or a toner/graphite powder. To improve the accuracy the speckle size is measured: usually it should be 3 or 4 times bigger than a pixel[8]. In this way it is possible to better check the speckle movements avoiding decorrelations or loss of information.
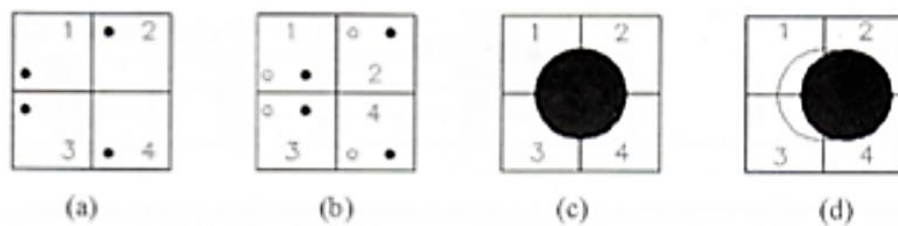

(a)   (b)   (c)   (d)

Figure 1.5.1-1: Speckle size: in the first case there isn't a brightness variation despite the speckle displacement due to the specimen deformation. In the second one, a good size speckle allows to measure its displacement.

The speckle size is calculated thanks to the ratio between the sensor pixels and the magnification factor which indicates how many pixels correspond to the unit length of the physical specimen[8].

$$M = \frac{ccd \; sensor \; bigger \; dimension \; [pixels]}{size \; computation \; window \; [mm]}$$

$$L = \frac{P}{M} \; [mm]$$

1.5.2 Correlation algorithm parameters

At this point it is necessary a calibration before starting the DIC correlation. A good choice of these parameters could reduce the noise, which is the DIC's principal error, allowing a good visualisation of strain gradients.

The correlation parameters are defined in order to obtain the best accuracy, precision and spatial resolution[9]; they are:

- Facet size: the images are divided in sub-images called facets[3] (N x N pixels); each of them is matched and correlated in all the frames taken to the specimen under load. The random pattern allows to distinguish every single facet because each of

them is identifiable thanks to the dot's dispersion. In this way the algorithm can recognise the specimen in all the frames because for each facet it calculates its frequency components; then the DIC software computes all the possible future frequency components due to load and compares them with the ones calculated of the following frame. The facet is recognised between two frames if there is a match. Its size is related to the dot's ones and influences accuracy, noise and the calculation time.

- Grid spacing it defines the overlapping between consecutive facets. It influences the computational cost but increases the precision and the accuracy of the strains calculated. It is reasonable using smaller grid spacing if high strain gradients are expected.

- Strain computation window: the displacements are derived to obtain strains; this operation increases the noise which is attenuated by a large strain computational window. On the other hand, this solution could reduce strain gradients effect.

- Filtering: it is used to reduce the noise due to the strain computation; this process has the same problem below described.

- Validity quote: it is a threshold for strain computing; it is linked to the valid points necessary to calculate the strain.
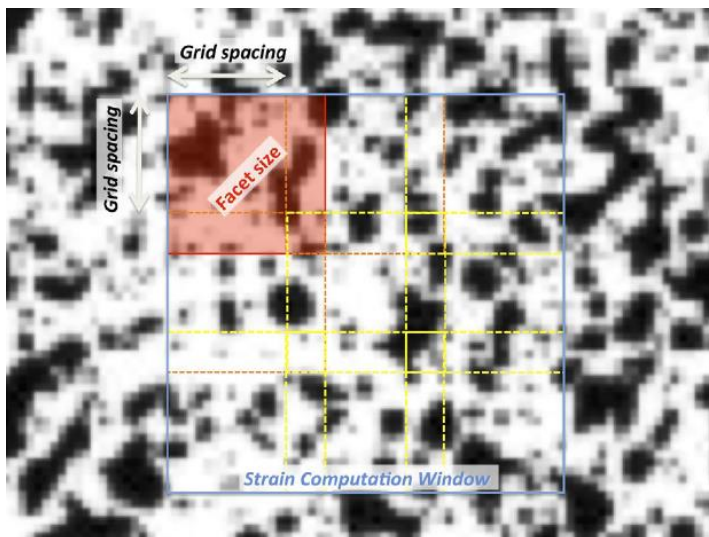

Figure 1.5.2-1: A visualisation of correlation parameters.

A big facet guarantees less noise, good accuracy but less local information. Conversely a little one is better to obtain local information, but it increases the noise

The DIC measurements are affected by various errors due to its process; generally, DIC computed strains are quite noisy, despite of a good accuracy[9]. To reduce errors some recommendations are observed, for instance the measurements are validated testing the DIC method on material with well-known properties.

There is no universally optimal set of the parameters[9] because the DIC method is used on a large quantity of cadaveric and in silico specimens with complex geometries; the specific application requires a certain choice of them. As explained before the choice of optimal parameters for the DIC allows to measure full field strain without any reinforcement of the specimens.

1.6 The aim

This work aims to obtain a first rib mechanical characterisation. In order to have a complete description, every single rib was studied through:

- loads and displacement values measured by the machine test;
- strains obtained thanks to DIC method;
- micro-CT scans to observe the internal structures.

Then the failure mode was investigated.

Chapter 2 – Material and methods

2.1 The specimens

Ninety-one ribs which came from 13 donators (7 male and 6 female) aged from 55 to 99 years were used for this study. Lateral and controlateral ribs from the fourth to the eighth position in the ribcage were taken, except some cases. The main reason for the ribs' choice is due to their frequent break in car accident or cardiac massages. Then were selected rib from the fourth to the eighth level.

The process can be explained through 4 steps

- Step 1: The selected ribs were cleaned, and their costal cartilages were cut off. In order to test only the calcified tissue, also the ribs ending were removed to eliminate all the possible cartilages components.
- Step 2: The ribs were aligned, and the extremities were immersed in PMMA like in the Figure 2.1-1.
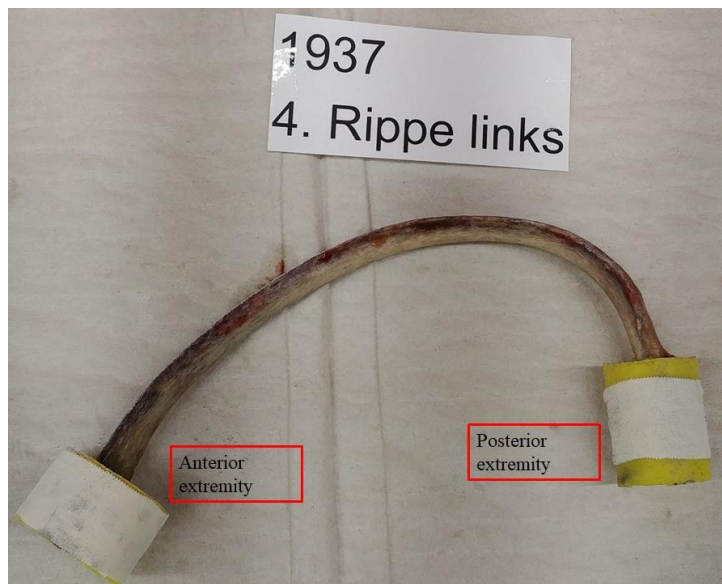

Figure 2.1-1: A tested rib.

- Step 3: A random speckle pattern was prepared on the ribs' surface to measure displacement and strain with DIC.
- Step 4: Each rib was positioned in the machine.

- Step 5: The test was performed.
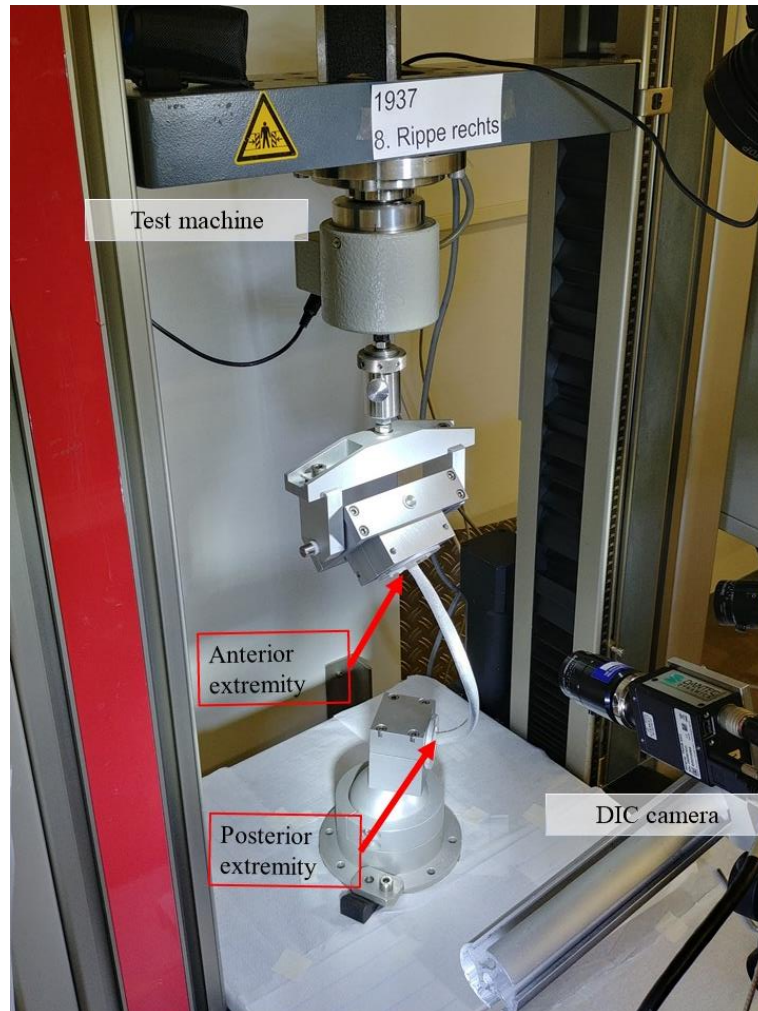- Step 6: Ribs were analysed with micro-CT scans.

Figure 2.1-3: Rib positioned in machine test.

Specimen no.	Sex	Age	Side	IV	V	VI	VII	VIII
Total			91	18	19	11	22	21
2150	male	81	Left	X	X		X	X
			Right	X	X		X	X
2151	male	91	Left	X	X			
			Right	X	X		X	X
2153	female	71	Left	X	X		X	X
			Right		X		X	X
1937	male	63	Left	X	X		X	X
			Right	X	X		X	X
2098	female	84	Left	X	X	X	X	
			Right	X	X	X	X	X
2149	female	99	Left				X	
			Right	X			X	
2097	male	96	Left	X	X		X	X
			Right	X	X		X	X
1806	female	55	Left			X	X	X
			Right					X
1717	male	80	Left	X	X	X	X	X
			Right	X	X	X	X	X
1410	female	64	Left			X	X	X
			Right				X	X
1810	male	62	Left	X	X	X	X	X
			Right	X	X	X	X	X
1808	male	68	Left	X	X	X	X	X
			Right	X	X	X	X	X
1820	female	65	Left		X	X		X
			Right					

Table 2.1.1: Ribs tested.

2.2 The test machine

A uniaxial testing machine (Zwick roll) was used in this study. The machine is able to applies a load on the ribs in order to create flexion on them. The posterior rib extremity was blocked in an interlock whereas the anterior one was inserted in a constraint with 2 degrees of freedom (dof). In this condition, the test was over constrained.

During the test the anterior end was moved to reach a defined displacement; as a consequence, the anterior end was bended causing traction on the external side and compression in the internal one.

Figure 2.2-1: The testing set.   *Figure 2.2-2: The force application.*
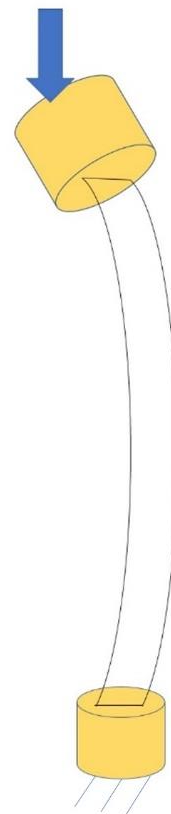
2.3 Global characterisation

Loads and displacement measured from the set up were saved in Excel files which were exanimated to obtain a global characterisation of the ribs.

Break load, stiffness and energy are obtained with a MATLAB script, called "summary_analysis" which uses 6 functions to select, organise and process the ribs data contained in the Excel files. Every rib is identified by a code that identifies the donor and the rib position in the ribcage. Each excel file contains several sheets in which are saved the calibrations parameter, the loads and displacements measured by the machine.

Initially the function "create_cell_array" creates 5 cell arrays where all ribs are collected. The ribs in each cell array are organised for their position in the ribcage. For this reason the cell arrays are called "rib_no4", "rib_no5", "rib_no6", "rib_no7" and "rib_no8"; in each column the "divide_number" function stores the rib's code, displacements and loads measured for each rib. Doing this every single column contains only the information about one rib.

In the next phase, all datas saved in a single cell array are given in input to "elaboration" and "mean_std_ks_test" functions; the first algorithm calculate the load and displacement break, the stiffness and the energy for each ribs and stores these values in the fourth, fifth, sixth and seventh lines of the corresponding columns. The second function manages to calculate mean and standard deviation of these values; subsequently it applies the Kolmogorov Smirnov test to break load, stiffness and energy mean in order to find out if these values follow a normal distribution. These data are given in input to another function called "one_way_anova_post_hoc": this algorithm implements analysis of deviance between the ribs' populations.

Finally, all the array tables are saved in the Excel file "Summary_Analysis" that contains one sheet per rib population and the last one, called "Summary" contains the mean and std values for each rib population about break load, stiffness and energy. These data are manually organised in another sheet called "Summary_Graphs" in order to obtain histograms which are useful for a better comprehension of the results.

The MATLAB script returns all the ribs' load-displacement graphs in 5 different images, one for population. There are also plotted the ANOVA tables calculated for the break loads, the stiffnesses and the energies.

This first analysis is useful to understand the differences between the ribs in the ribcage: the results are shown in "First analysis" section of the chapter "Results". During these elaboration each ribs' load-displacement graphs were observed and were removed the ones that had problems during the test; for this reason, 12 ribs were removed.
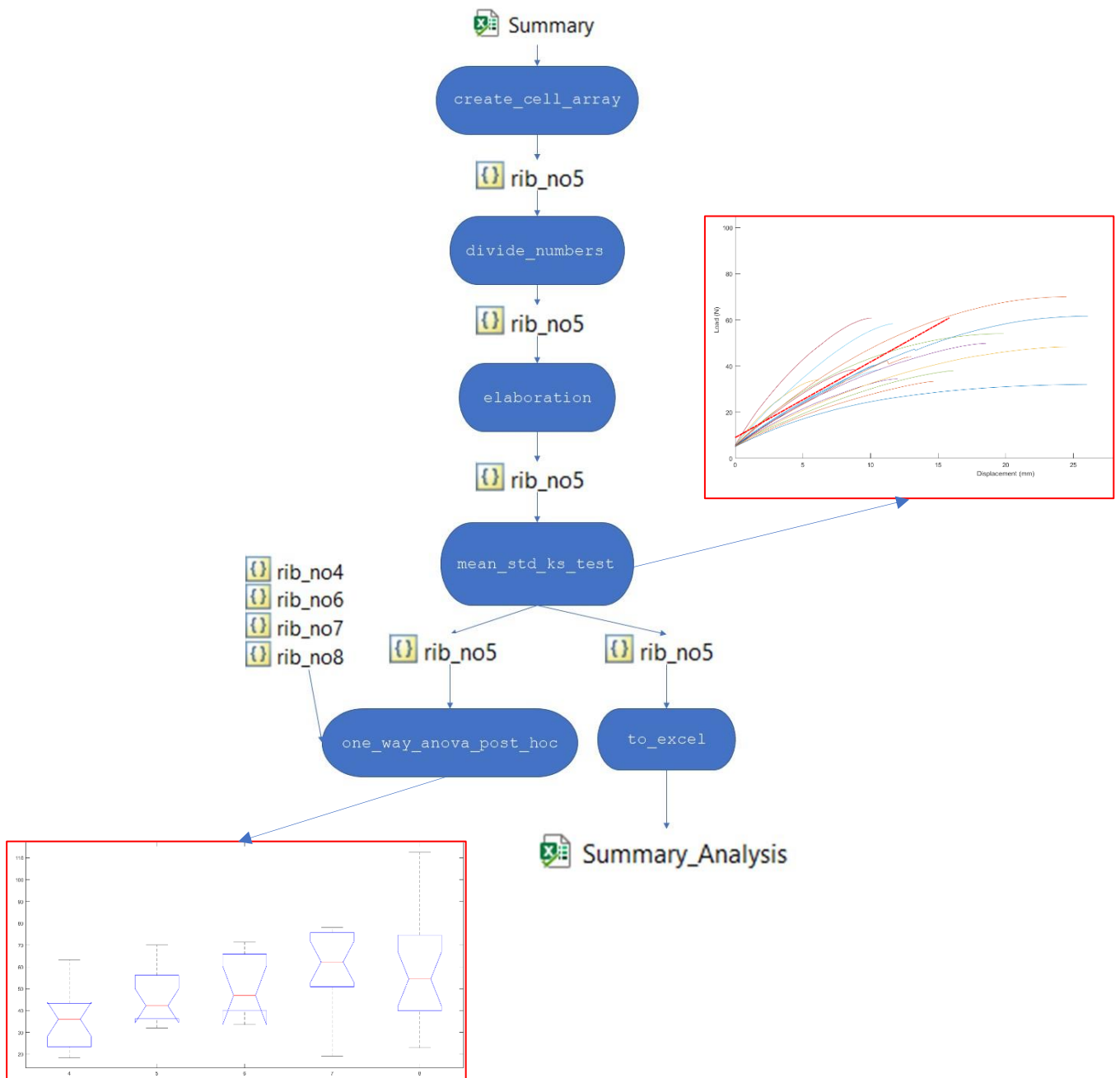
Figure 2.3-1: summary_analysis workflow for fifth ribs.

2.4 DIC instrumentation

In front of the machine, there is all the DIC system.

The DIC instrumentation consists in:

- Two high speed cameras: they are positioned in front of the set-up to obtain a proper 3D visualisation of the surface. The digital images acquired are subjected to random errors due to the camera's technology and the out-of-plane displacement of the specimen during the loading[9]; this one can be avoided with preliminary tests;
- Data box to synchronize the testing machine measurements;
- Halogen or led white light system: a proper illumination guarantees a good recording avoiding light reflection;
- Computer for image correlation and elaboration.

The machine allows to show both ribs sides.

The correlations parameters are set in this way:

- Facet size: 30 pixels;
- Grid spacing: 50%/70% facets area;
- Filtering: local regression from 11x11 to 17x17.

In order to study the strains, the images acquired with the digital image correlation are processed in "Istra 4D V4.3.1" (Dantec Dynamics, Skovlunde, Denmark)

Each specimen recording is composed by two files called "noise" and "failure"; the first allows to set the correlation parameters. Indeed this file is constituted by only the reference frame: in principle any strain could be calculated because the load is not applied. However the software computes strains because the correlation parameter are not set. A good correlation is possible if the reference step does not show any strain. The "failure" file permits to calculate the strains at the break point. Despite these two files, the "failure" file allows both the operation below described.

To start the correlation is necessary to set the appropriate parameters in the following sections:

- Mask definition: here there are the first settings to deal with. The "mask" button allows you to define the area on the specimen to study; in this Thesis the mask

covers all the specimen surface visible where is possible. Then it is possible to define a point to start the correlation.

- Startpoints: in this section the software identifies the start point for all the steps.
- Evaluation settings: here it is possible to define the facets dimensions and the grid spacing: usually the facet dimensions are based on the dot size and the overlap is the 50-70% of facets' area.

Finally, the images acquired are completely correlated and it is possible to work on them clicking on "Control".

In this section there are several measurements in order to satisfy every user request. In this Thesis the strain gradients long the principal directions (eps1, eps2) and ɣ for each rib are observed. A scale from -15000 to 15000 µℇ was used for a better visualisation of the strain gradients.

Some ribs (11) were not correlated due to excessive light reflections or correlations problem that disturbed the software process.
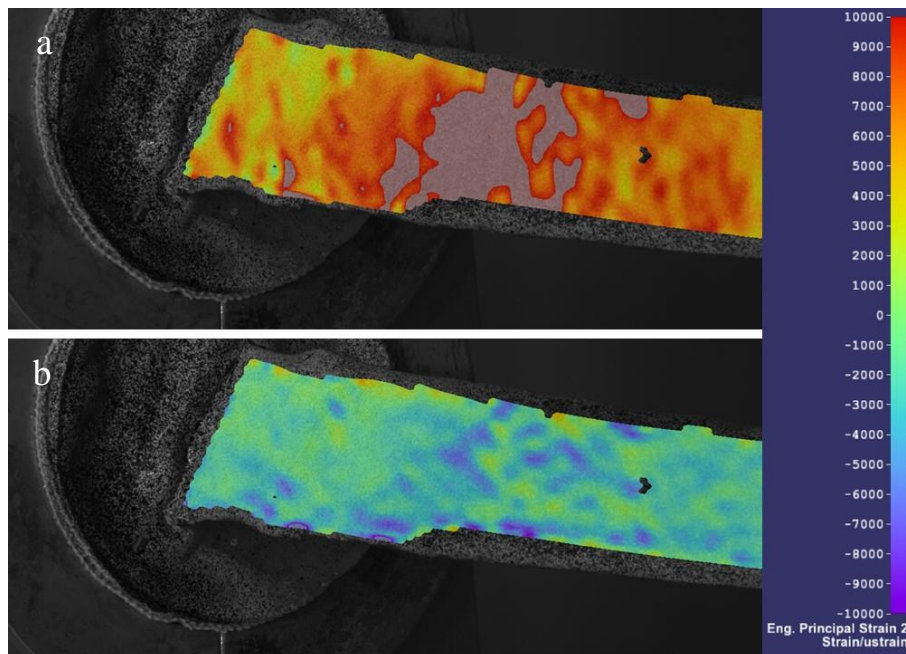
Figure 2.4-1: This is a strain visualisation of a fourth rib (1717_4l); the maximum strains (a) and the minimum strains (b) are represented. Initially a scale from -10000 µℇ to 10000 µℇ was used. In this way higher strains values could not be observed (a).

31

2.5 Statistical Analysis

In order to study 89 specimens, it is necessary to use some statistics concepts to obtain a proper analysis.

All the analysed groups follow a normal distribution. To recognise if a group follows a normal distribution, the "Kolmogorov-Smirnov test" is used. A MATLAB function called "kstest", is able to compute this task and checks that every group tested with ANOVA follows a normal distribution.

ANOVA stands for "Analysis Of VAriances": it explains if the differences between groups are due to statistic errors or the groups belong to populations with different means.

Here it is reported the ribs' break load analysis to understand the one-way ANOVA method.

As explained in the subchapter "The specimen" the ribs differ each other for their position in the ribcage. Therefore there are 5 ribs groups. For every rib, the break load is computed. Subsequently for each rib group it is possible to calculate their sample means.

Ribs	Mean/Std	Rib 4	Rib 5	Rib 6	Rib 7	Rib 8
Break (N)	Mean	35,14	46,03	52,00	59,19	59,67
	Std	12,55	11,91	14,42	17,47	25,21

Table 2.5-1: Break means and standard deviations of all the rib levels.

The aim consists in understanding if there are differences between the five groups excluding statistic errors. Thus there are 2 hypothesis:

- Null hypothesis: the 5 populations have the same means. $\mu_0 = \mu_1 = \ldots = \mu_N$.
- Alternative hypothesis: at least, one population mean differs from the others.

In order to confirm one of these hypotheses, it is mandatory to distinguish the variances inside every groups and the ones between groups. Here there is the definition of variance (s^2).

$$s^2 = \frac{\sum_{i=1}^{n}(x_i - \overline{x})^2}{n - 1}$$

x_i is a sample value, $\overline{x}$ is the sample mean and n is the quantity of samples.

The variance within groups is the ratio between the sum of deviances for each group and the sum of the degrees of freedom (#observation-#groups).

$$MSW = \frac{\sum_{i=1}^{n}(x_i - \overline{x})^2}{\#observation - \#groups}$$

observation are all the samples of all groups.

The variance between groups is the ratio between the sum of deviance per number of samples for each group and the degrees of freedom (#groups-1).

$$MSB = \frac{\sum_{i=1}^{n}(x_i - \overline{x})^2 \cdot n_i}{\#groups - 1}$$

The ratio of the two variances is equal to F number.

$$F = \frac{MSW}{MSB}$$

This value assumes a meaning if we consider an F distribution that is the ratio variances trend. The F distribution depends on the ratio between the MSB degrees of freedom and the MSW ones. For every F number is possible to compute its probability considering the underlying area until the F calculated. At this point it is useful to compare the F value with a critical F value (F_α) which depends on the significance level (α). The significance level is the probability to confirm or reject the null hypothesis; usually is equal to 5%. This means that if we consider the null hypothesis true, it will be a probability less than 5% to reject the null hypothesis.
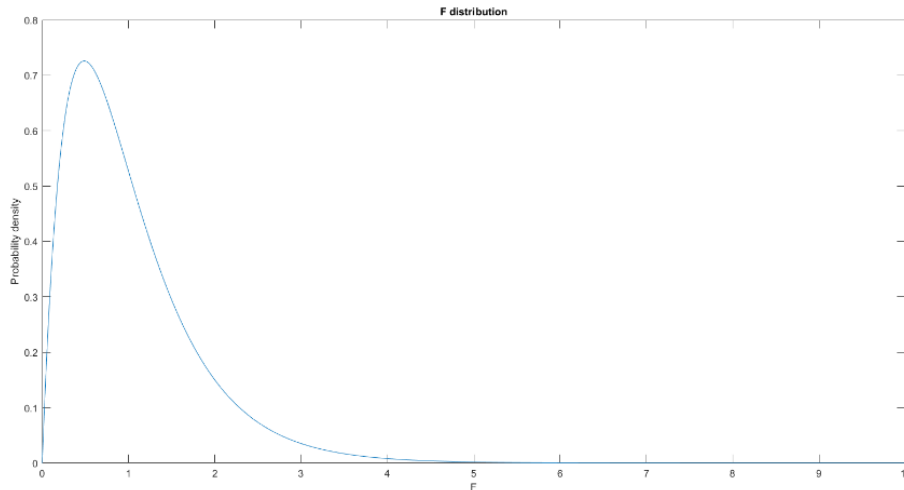
Figure 2.5-1: A F distribution. On x axis there are the F numbers whereas the y axis represents the probability density. This F distribution was computed using MSB degrees of freedom=4 and MSW degrees of freedom=72.

The comparison between the F value and F_α allows to accept or reject the null hypothesis:

- If $F < F_\alpha$, the null hypothesis is confirmed. As a consequence $\mu_0 = \mu_1 = \ldots = \mu_N$
- If $F > F_\alpha$, the null hypothesis is rejected. At least, one population mean differs from the others.

If the second case occurs, the differences between groups are confirmed; on the other hand ANOVA does not specify which groups differ from the others. In order to find them, the "post hoc" analysis is computed. It returns the groups that differ significantly from the others. This task it is possible thanks to a MATLAB function called "multcompare".

2.6 Micro-CT scan

The micro-CT scans allow to study the bone microstructure. Here a brief description is provided.

Micro-CT is a kind of computed tomography which allows to study microstructures with a high resolution. The computed tomography (CT) uses the x-rays to obtain a bidimensional projection of 3D structures. There are several type of CT systems, but the physics principle are the same. Indeed, the CT scanners have an x-ray source and a detector in front of it: among them the broken rib is positioned. The source produces the x-rays which pass through the ribs; according to their nature x-rays are absorbed by the material that are

crossing. The absorption depends on the material density: a high-density material absorbs more x rays than a less density one. In this way it is possible to distinguish different tissues. As a consequence, the detector will receive the non-absorbed x-rays. Through back projection algorithms, it is possible to know the material density by comparing the x-rays produced and the received ones. This procedure is repeated more times by turning the x-ray source and the detector around the rib. In this way it is possible to have a complete visualisation of the section analysed, called "slice". In the CT scan, materials which absorbed more x-rays are the whiter ones whereas the materials that absorbed less x-rays are the darker ones.

The micro-CT scans were acquired in Germany through "Skyscan 1172" (Bruker, Ettlingen, Germany) using the software "Skyscan 1172 MicroCT" (version 1.5), with a camera resolution of 11,57 $Pixel/\mu m$. Through the "ct_comparison" Matlab script, each micro-CT scan is associated with the corresponding rib and the $\frac{Bone\ volume}{Tissue\ volume}$ are saved in the cell arrays produced by "summary_analysis" algorithm.
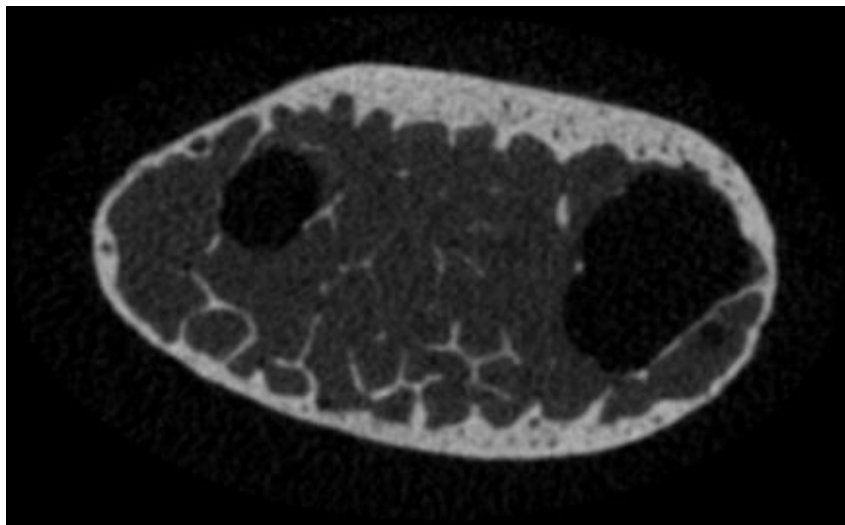
Figure 2.6-1: A rib micro-CT scan.

Chapter 3 – Results

As explained before, 89 ribs were tested: 11 specimens slipped during the test or the recording wasn't performed at the same time of load application. Other 11 ribs were not correlated for optical issues like light reflection or high strains errors.

During the tests the ribs broke in three different ways:
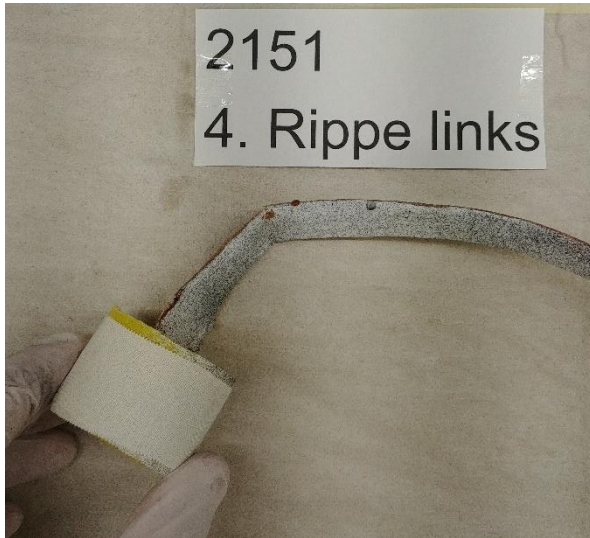
Figure 3-1: A "ductile" break: this rib collapse as a "straw".

- Horizontal fragile fracture: it occurred for 31 ribs. In particular 11 ribs broke in the external side whereas 20 ribs broke in the interior one.
- Longitudinal fragile fracture: only 5 ribs broke in this way.
- "Ductile" fracture: it occurred for 30 ribs. In this case, "ductile" word is used to describe a sort of "straw effect" shown in the Figure 3-1.

All the fractures occurred near the anterior rib extremity, only one occurred near the posterior extremity. Several ribs broke in the connection between the rib anterior extremity and the 2 dof constraint.

The following paragraphs describe the failures from the global view to the local one and finally there is the comparison with the micro-CT scans.

3.1 Global analysis

The global analysis allows to compare the different ribs groups in terms of break load, stiffness and energy. The "Kolmogorov Smirnov" test confirmed that all the values studied belong to normal distributions.

Ribs	Mean/Std	Rib 4	Rib 5	Rib 6	Rib 7	Rib 8
Break (N)	Mean	35,14	46,03	52,00	59,19	59,67
	Std	12,55	11,91	14,42	17,47	25,21
Stiffness (N/mm)	Mean	2,53	3,27	3,98	4,87	4,35
	Std	0,86	1,27	1,70	1,33	1,48
Energy (N·mm)	Mean	331,33	512,82	532,16	555,08	658,52
	Std	186,72	316,69	406,48	365,49	462,69

Table 3.1-1: Break, stiffness and energy means and standard deviations of all the rib levels.

As the Table 3.1-1 explains, it is possible to recognise an increasing trend for the break load and the energy for lower ribs. The stiffness follows the same trend until the seventh ribs. The ANOVA method and the post hoc analysis produced the following results:

- Break load: each rib group has 5 different break load means. ANOVA confirmed the existing differences between the 5 break load means; post hoc analysis points out that only the fourth rib values differs significantly from the seventh and the eight ones.
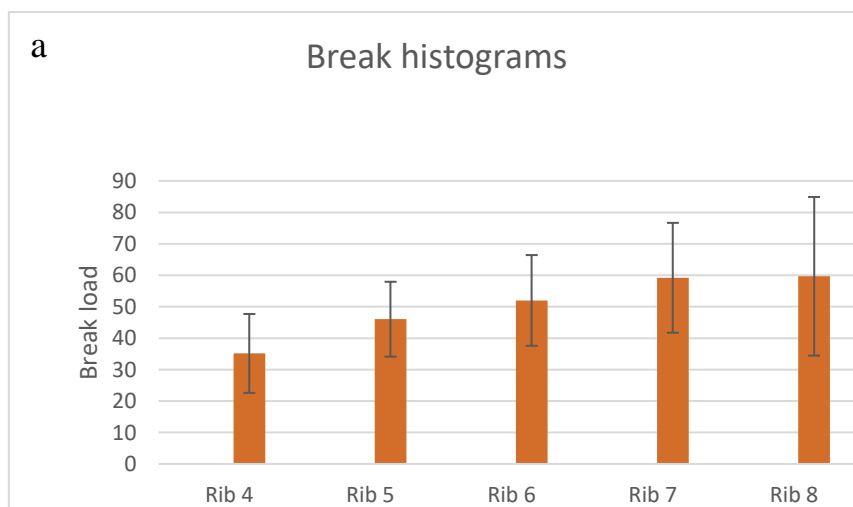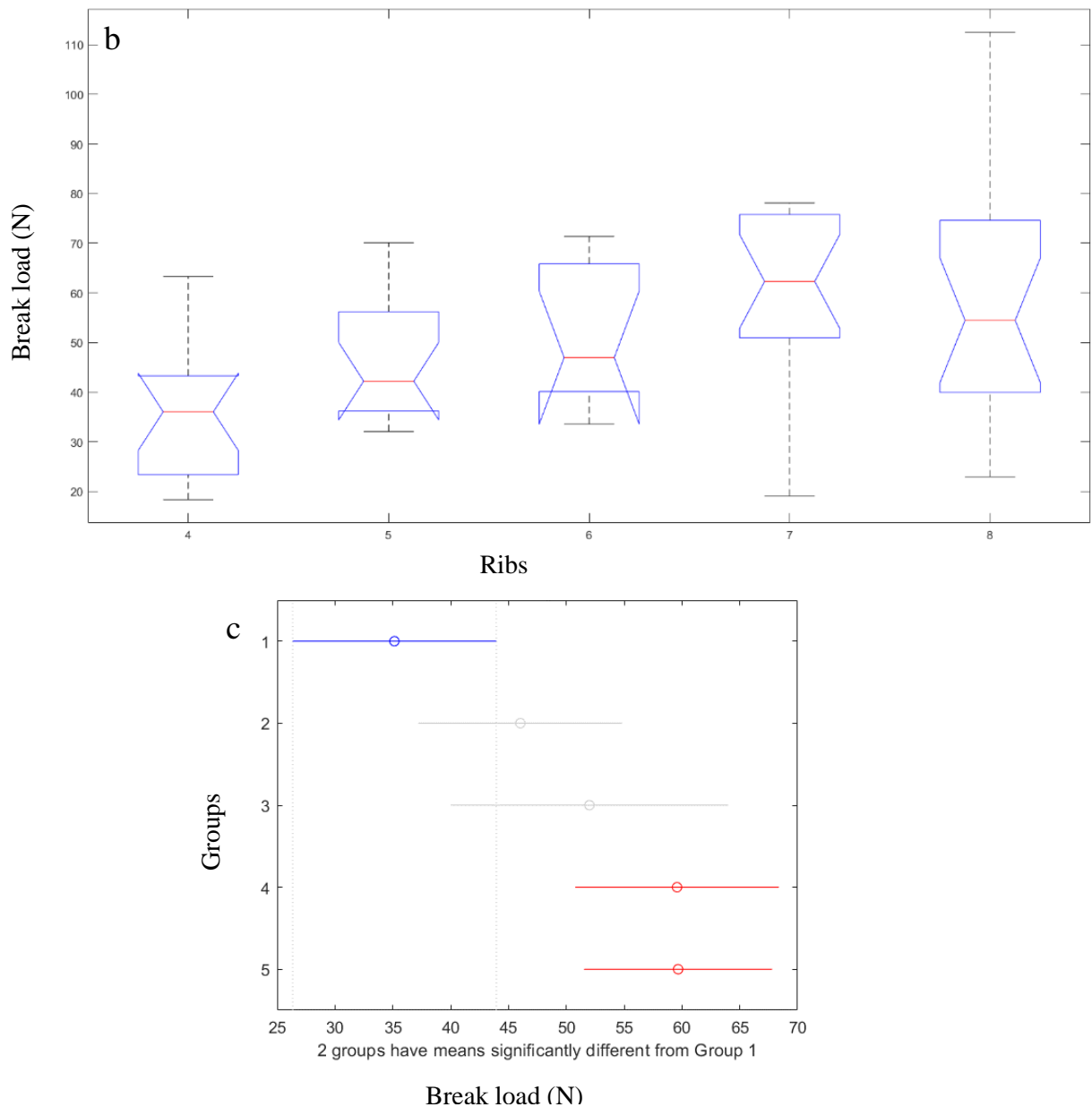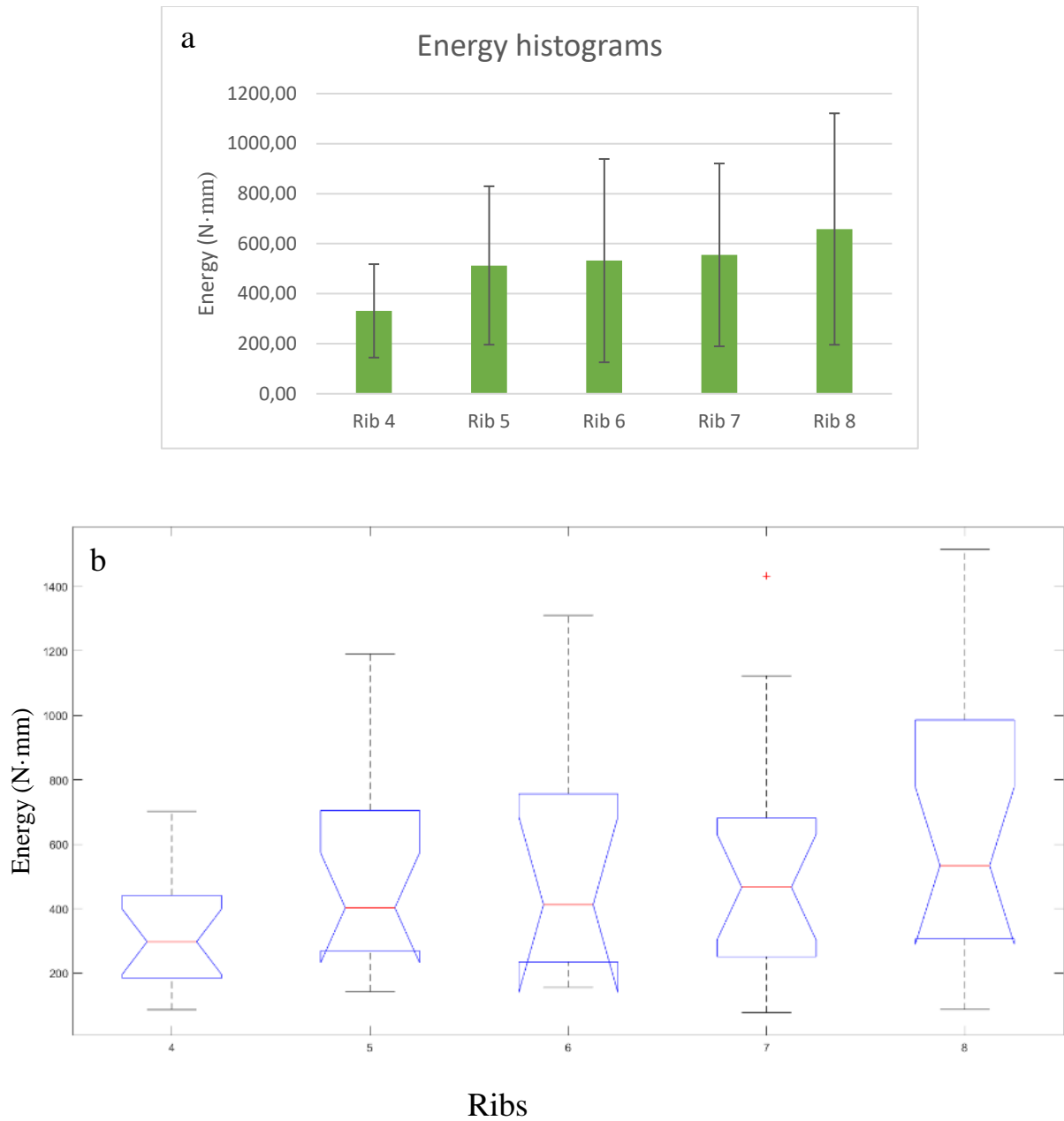
Figure 3.1-1: The break analysis: from (a) it is possible to observe a trend between the break load and the rib level. ANOVA partly confirmed this trend (b and c).

- Stiffness: each rib group has 5 different stiffness means. ANOVA confirmed the existing differences between the 5 stiffness means; post hoc analysis points out that only the fourth rib values differ significantly from the seventh and the eight ones.
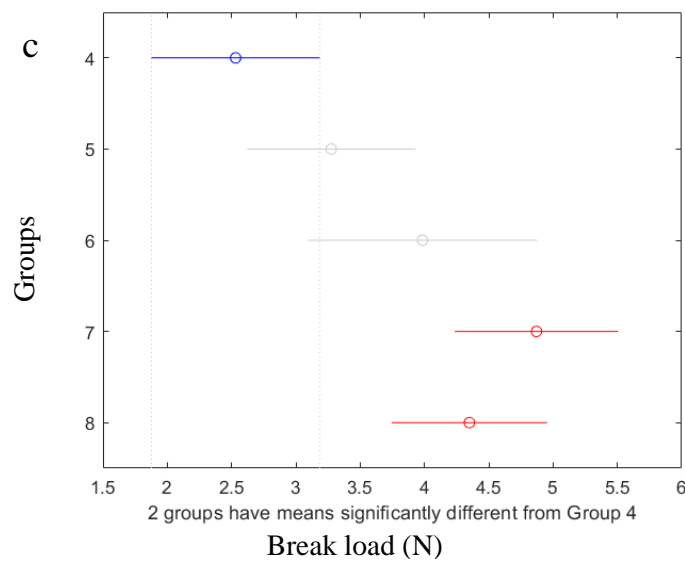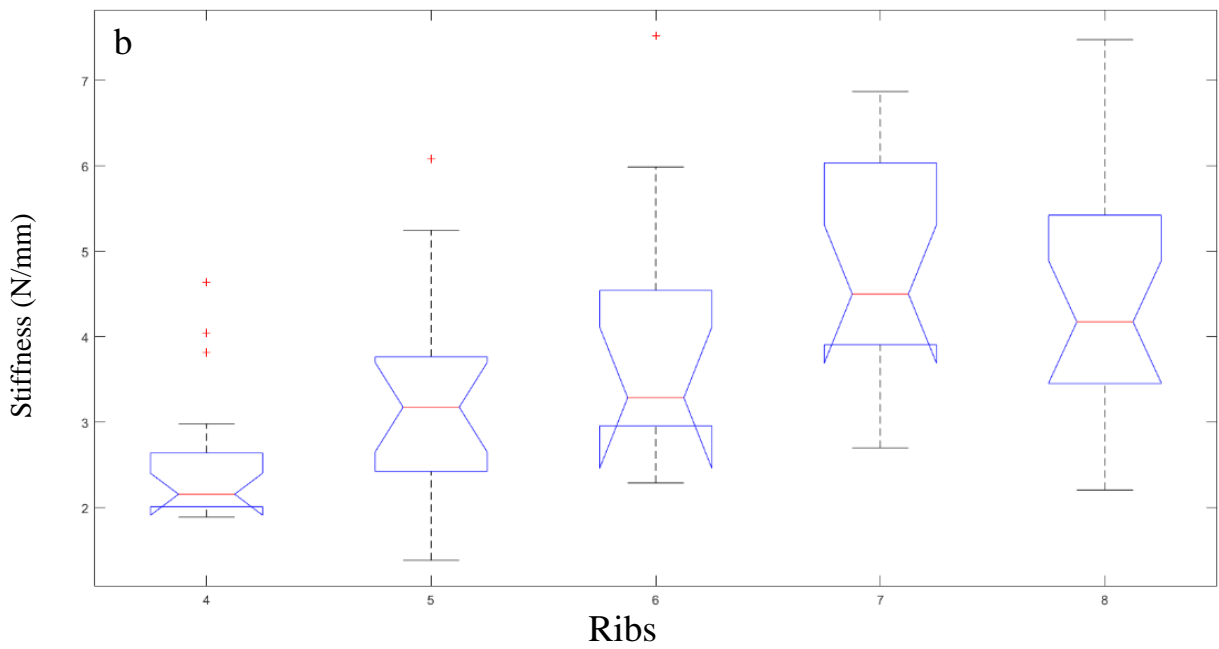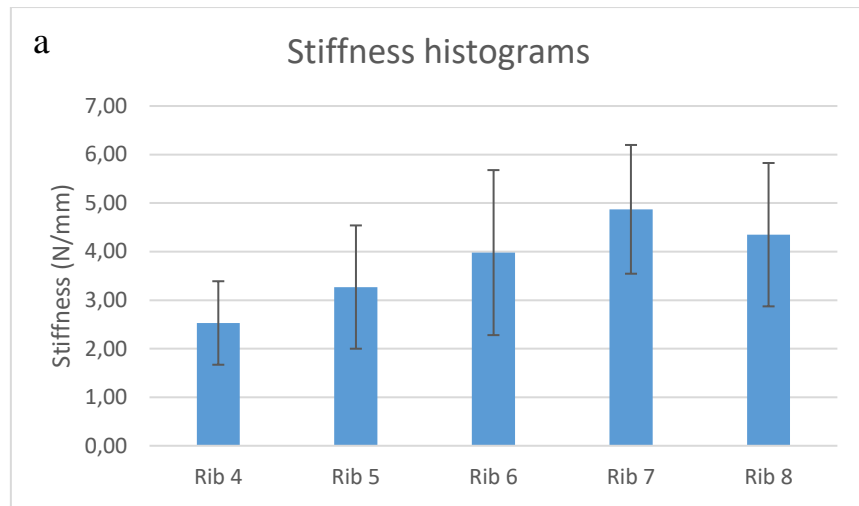
Figure 3.1-2: The stiffness analysis: from (a) it is possible to observe a trend between the stiffness and the rib level. ANOVA partly confirmed this trend (b and c).

- Energy: each rib group has 5 different energy means. ANOVA points out that the energies between rib groups do not differ.

Figure 3.1-3: The energy analysis: from (a) it is possible to observe a trend between the stiffness and the rib level. ANOVA did not confirm this trend (b).

3.2 Local analysis

The DIC method computes the strains on the external side and on the internal one thanks to the set up.

- External side: the maximum strains (ε_1) measured are directed along the longitudinal rib axis; according to the Mohr's circle, the minimum strains (ε_2) are perpendicular to the longitudinal axis. The ε_1 strains result higher near to the break point. Usually the ε_1 strains increase if the break load is higher. The same occurrence is shown by the ε_2 strains: in particular ε_2 strains increase if the break occurs in the other side. In modulus, $|\varepsilon_1| > |\varepsilon_2|$.
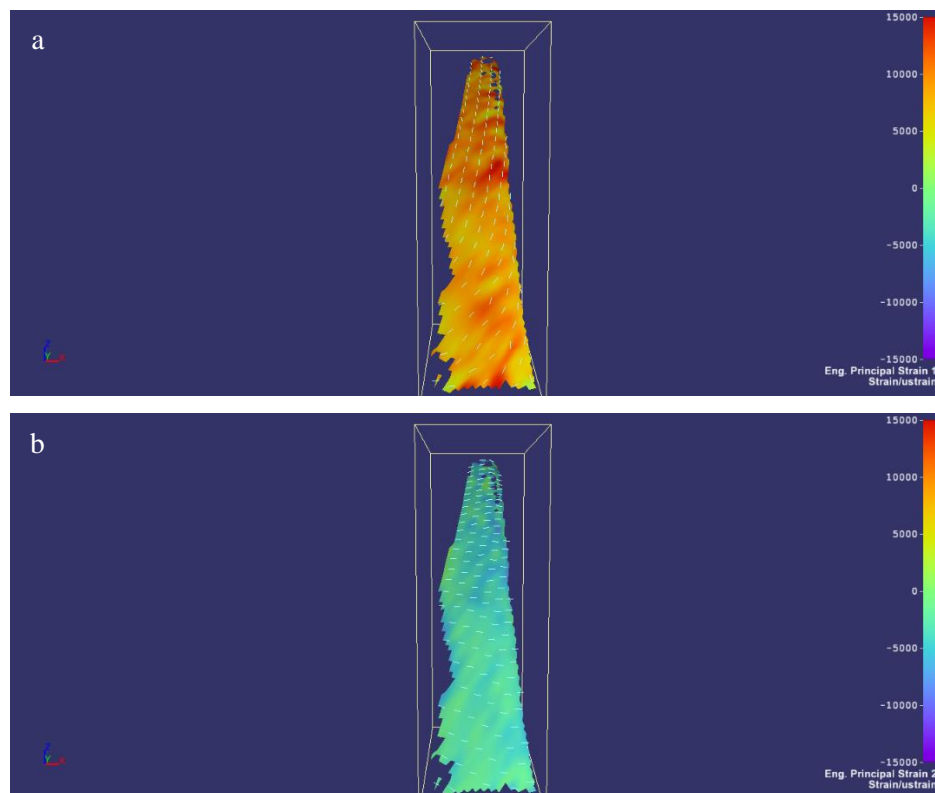
Figure 3.2-1: In this figure the maximum (a) and minimum (b) strains for 1808_4l are represented. It is an external view.

- Internal side: for this view, the correlation was difficult because several times the ribs surface was covered by the machine (Figure 3.2-2). Like on the external side, $|\varepsilon_1| > |\varepsilon_2|$ but with different direction. Indeed ε_1 strains are perpendicular to the longitudinal rib axis whereas ε_2 strains are directed along the same axis.
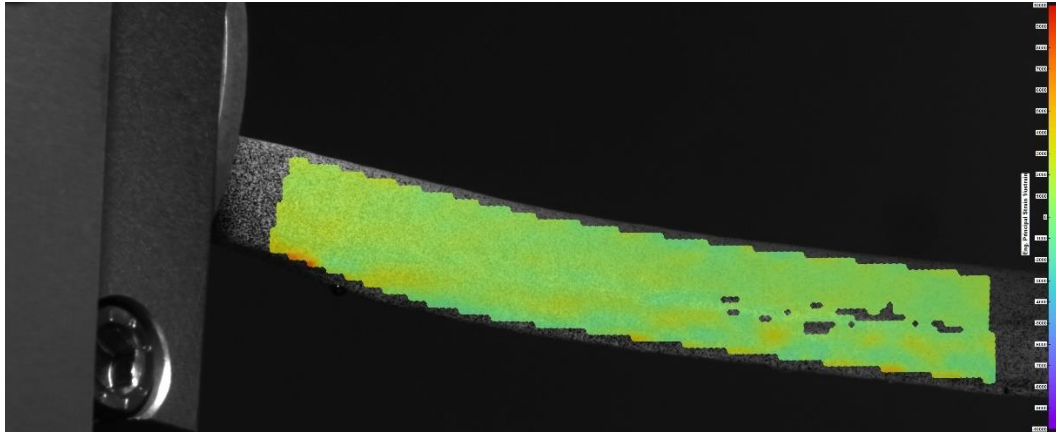
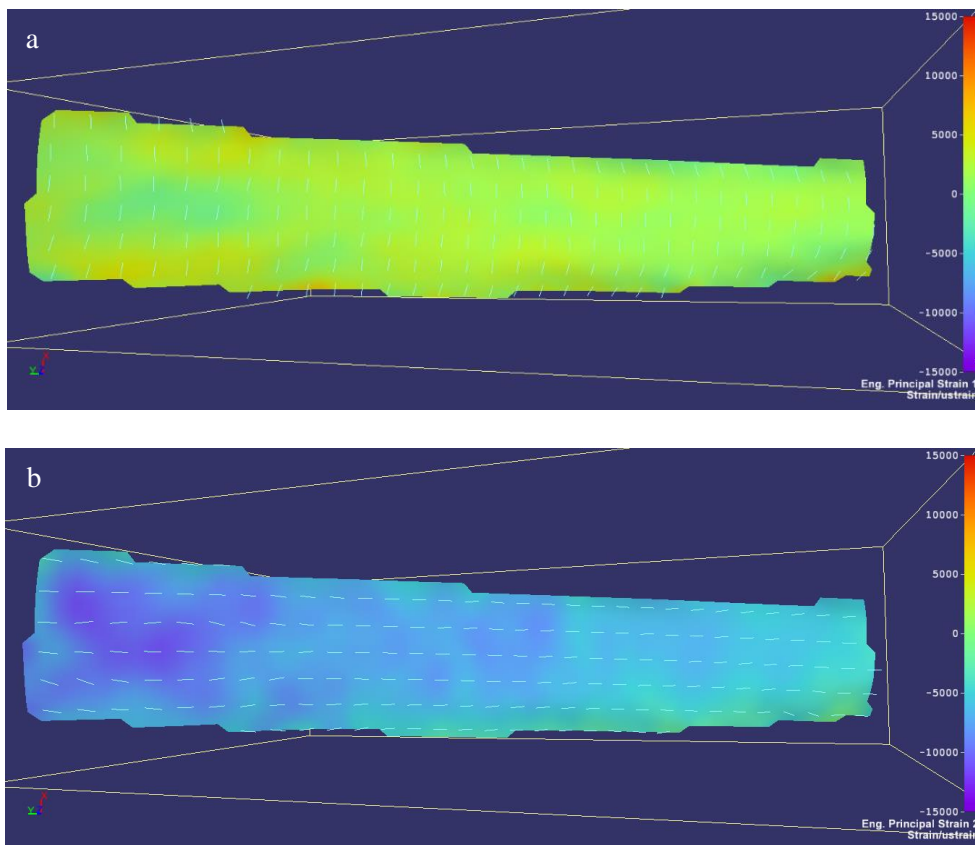*Figure 3.2-2: In this image it is possible to observe that the machine is covering the rib (1806_8r) visual.*

Figure 3.2-3: In this figure the maximum (a) and minimum (b) strains for 1808_6r are represented. It is an internal view.

Generally, $|\varepsilon_1|$ and $|\varepsilon_2|$ strains measured on the external side result bigger than the $|\varepsilon_1|$ and $|\varepsilon_2|$ of the internal one.
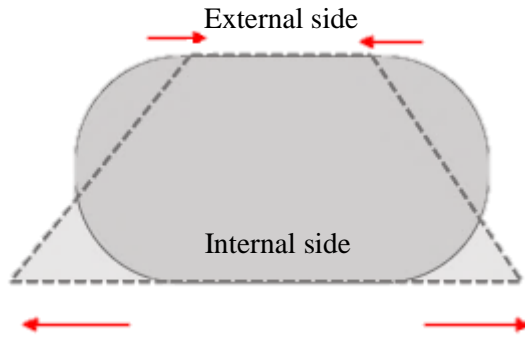
Figure 3.2-4: This is a rib section representation. During the tests, the external side decreases its width and increases its length. Meanwhile, the internal side increases its width and decreases its length.

In addition to $|\mathcal{E}_1|$ and $|\mathcal{E}_2|$, the γ is measured for each rib. Through the Mohr's circle, the ϑ angle is computed.

Observing all the ribs, it is possible to notice that the values of γ and ϑ assume values different from 0. The angle-break load graphs are represented for each kind of fracture and for every rib group.
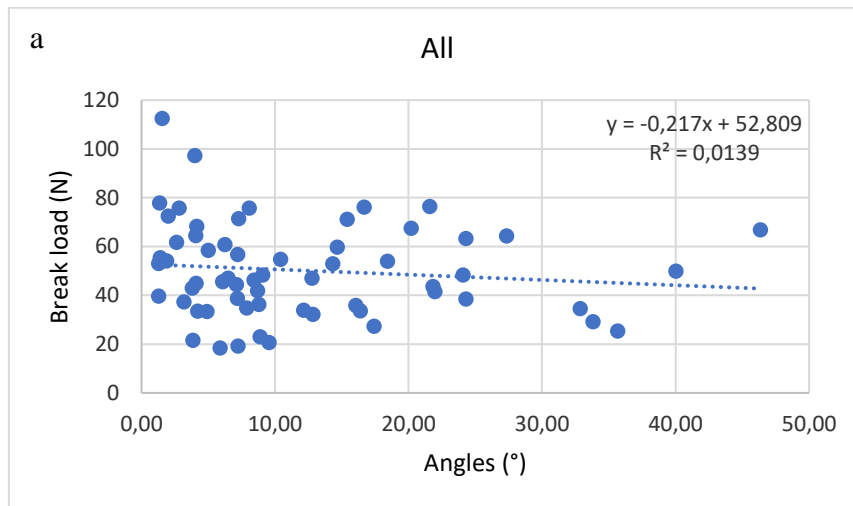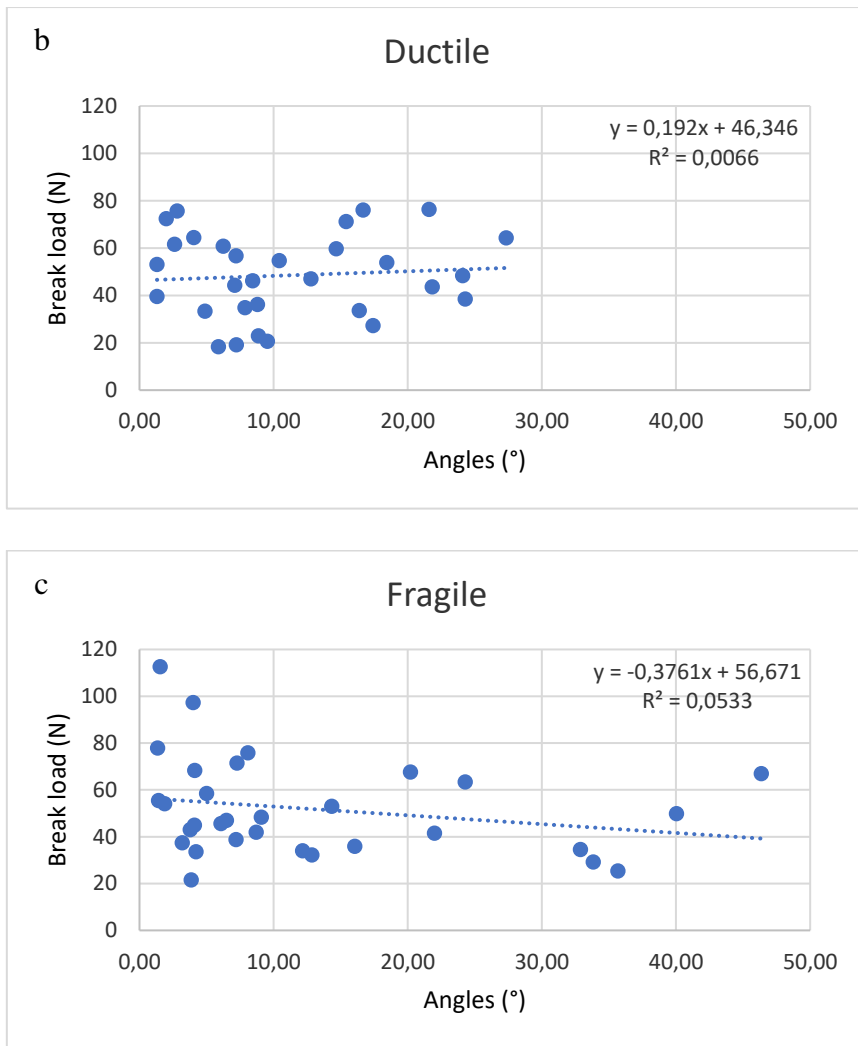
Figure 3.2-5: In these images are represented the relationships between break loads and angles. The angles are in absolute value.

It is not possible to find a particular relationship between the kind of failure and the angles measured. It seems that higher angles are calculated on ribs which break load (both ductile and fragile failure) belong to a range of 40 to 70 N; these values are reached by ribs from the fifth to seventh position in the ribcage. This behaviour could be confirmed observing the break load- angle graphs for each rib group.
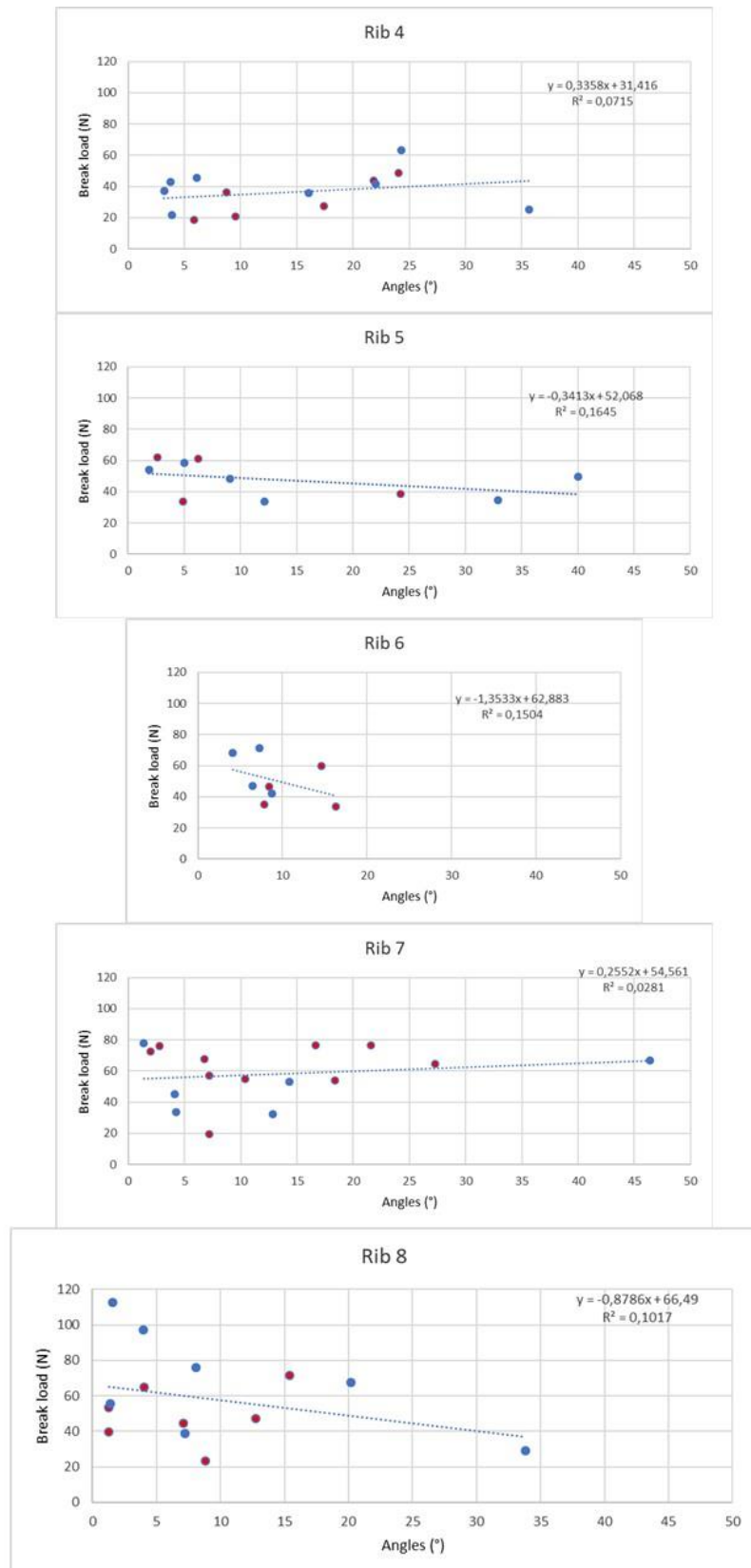
Figure 3.2-6: The blue dots represent fragile fracture, whereas the red point the "ductile" one.

3.3 Micro-CT comparison

Thanks to the MATLAB script "ct_elaboration" it is possible to link the break load and the stiffness with the percentage $\frac{Bone\ volume}{tissue\ volume}$. ANOVA test was performed to check the differences of bone density mean between the groups; the means do not differ significantly.
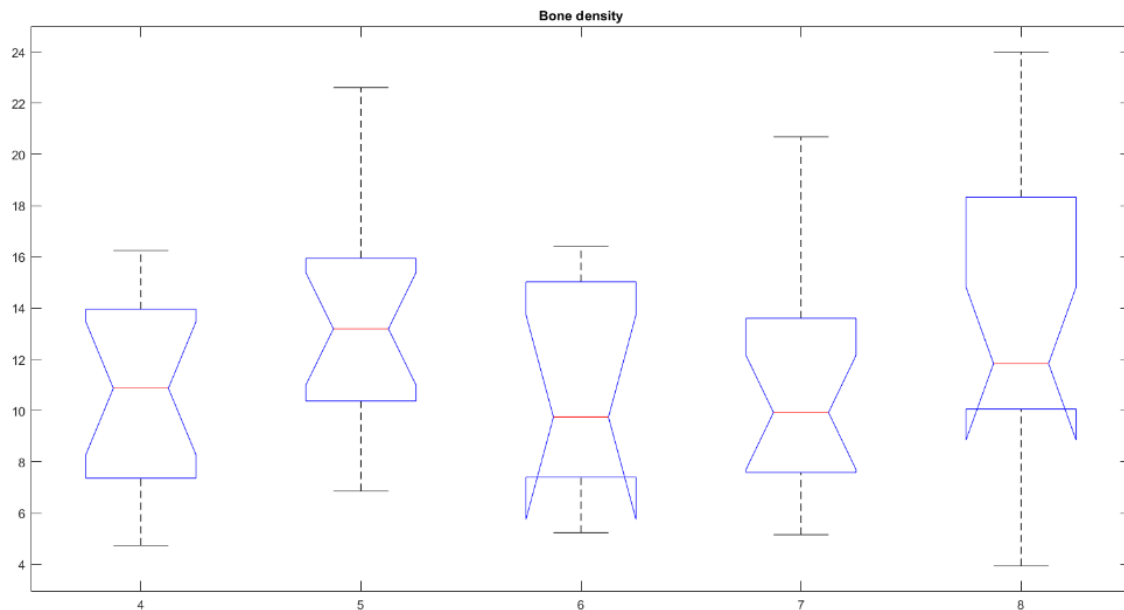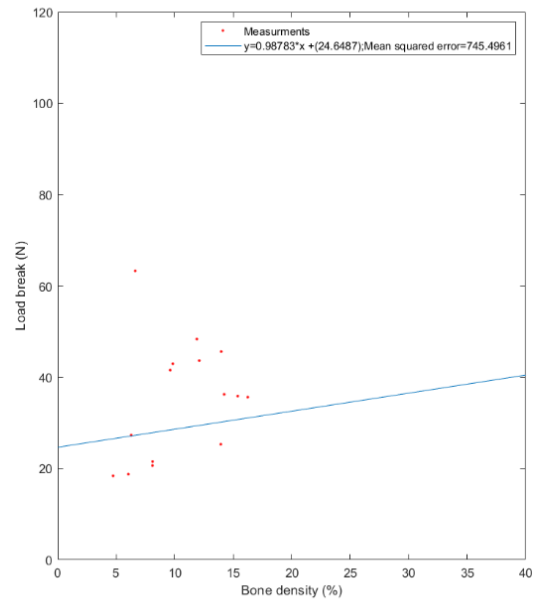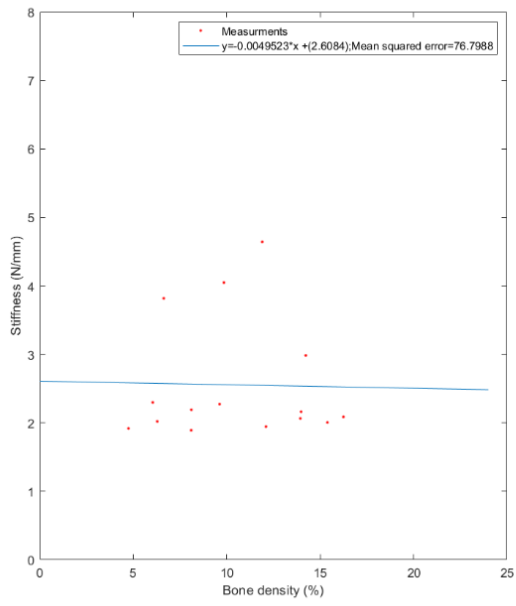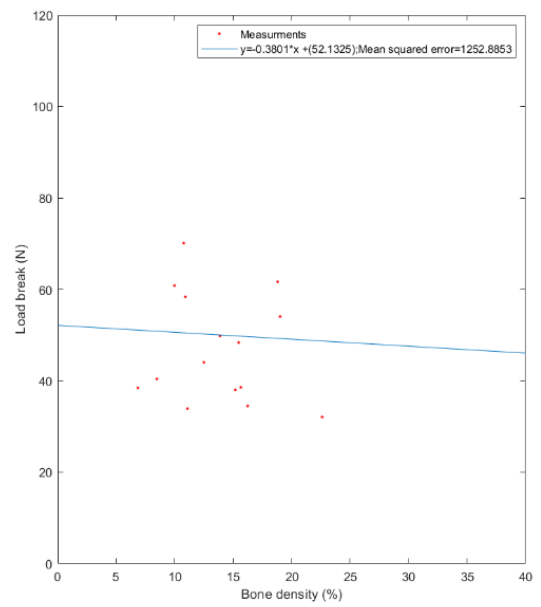

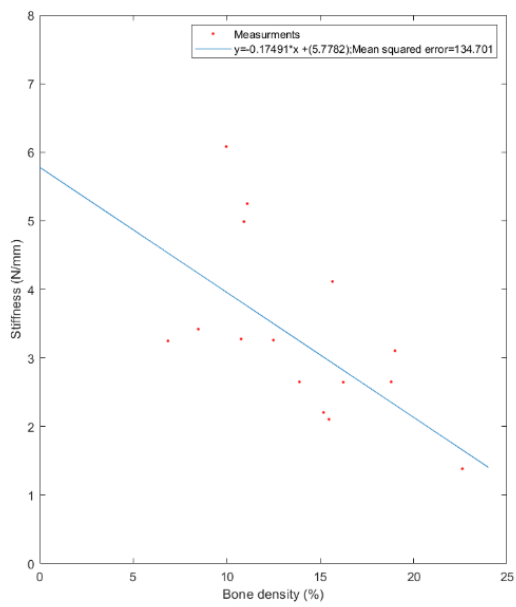*Figure 3.3-1: Bone density boxplot.*

The break load increase with the $\frac{Bone\ volume}{Tissue\ volume}$ (except for the fifth rib): this is confirmed by the interpolation (the blue line). It is possible to observe that lower stiffnesses occur in ribs with higher values of $\frac{Bone\ volume}{Tissue\ volume}$ volume, except for the eight ones.
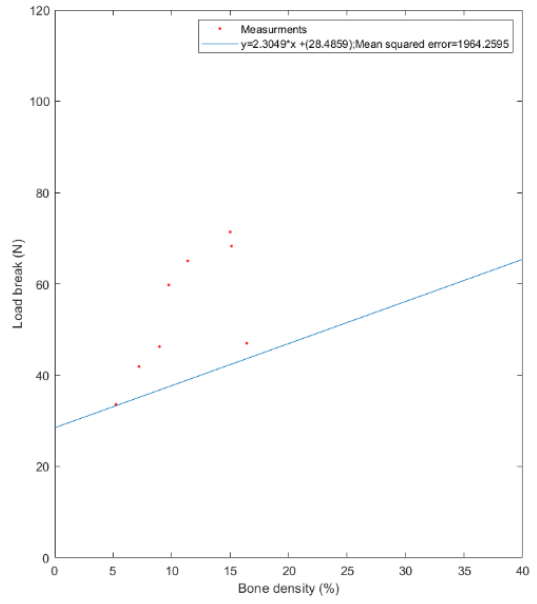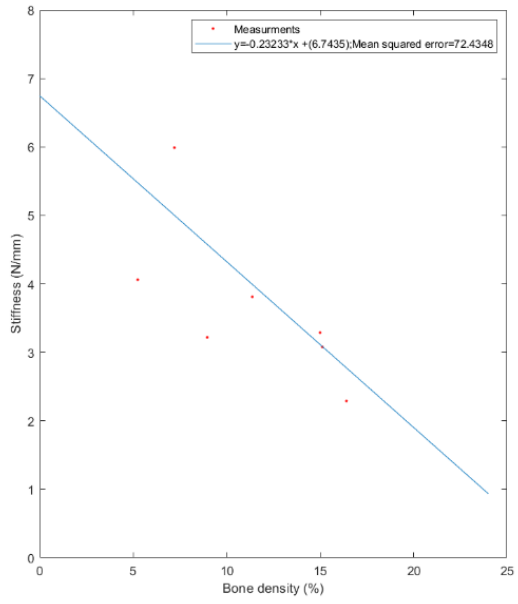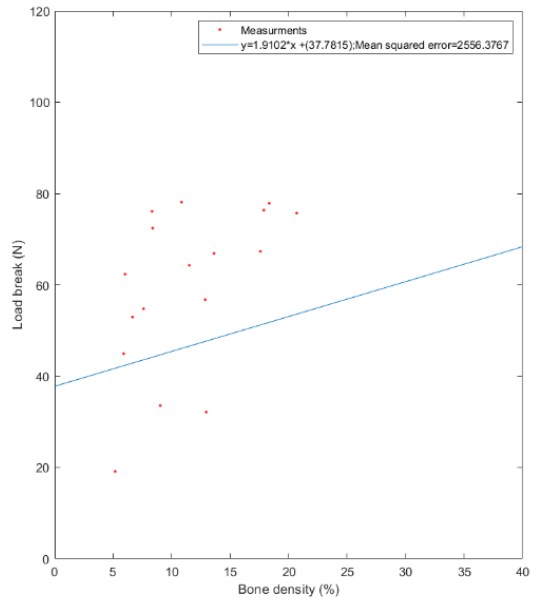
Rib number 4

Rib number 5

Rib number 6

Rib number 7
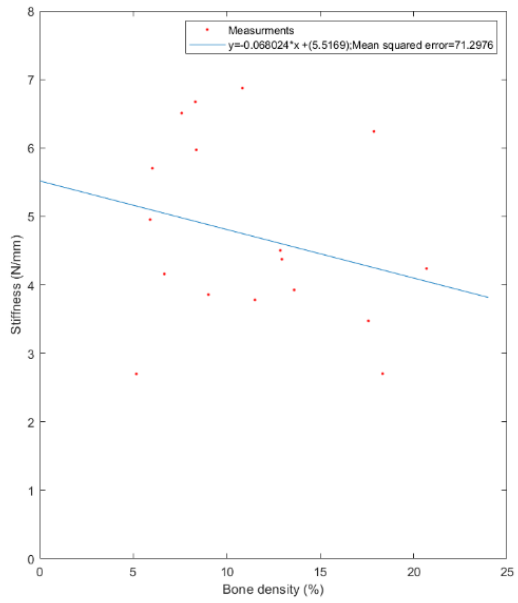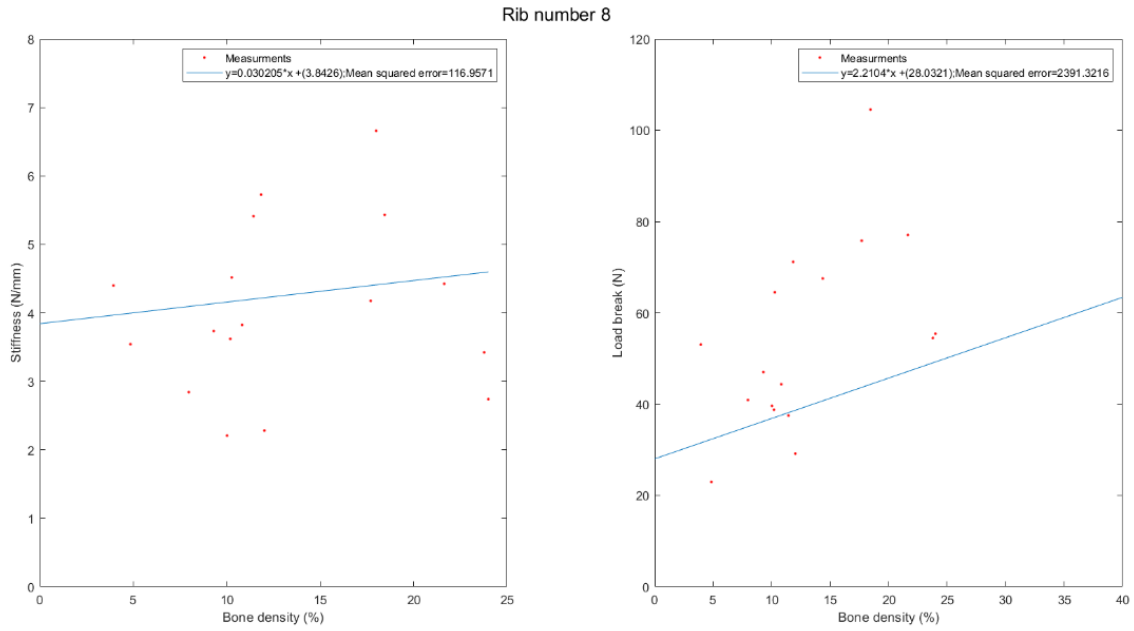
Figure 3.3-1: These are the graphs of load vs $\frac{Bone\ volume}{Tissue\ volume}$ and stiffness vs $\frac{Bone\ volume}{Tissue\ volume}$ for each rib.

In order to have a complete description, each load-displacement rib graph is associated with the corresponding micro-CT scan.

The micro-CT scans are compared with each rib break and stiffness values. It seems that, within groups, the break load is bigger in ribs with a lot of tissue (both calcified and soft). On the other hand the stiffness increases if the trabecular tissue is remarkable.
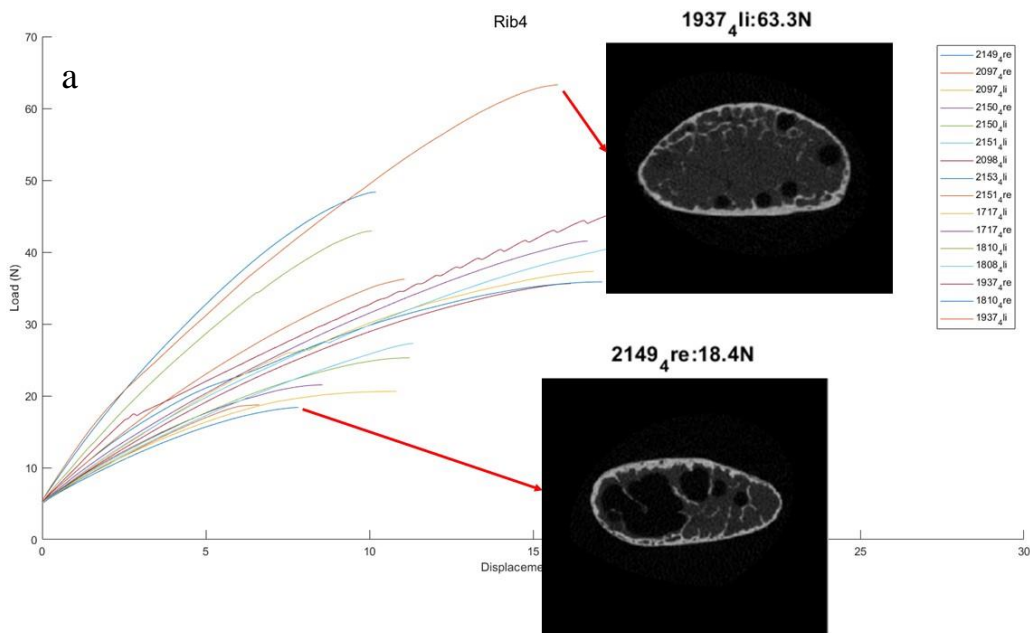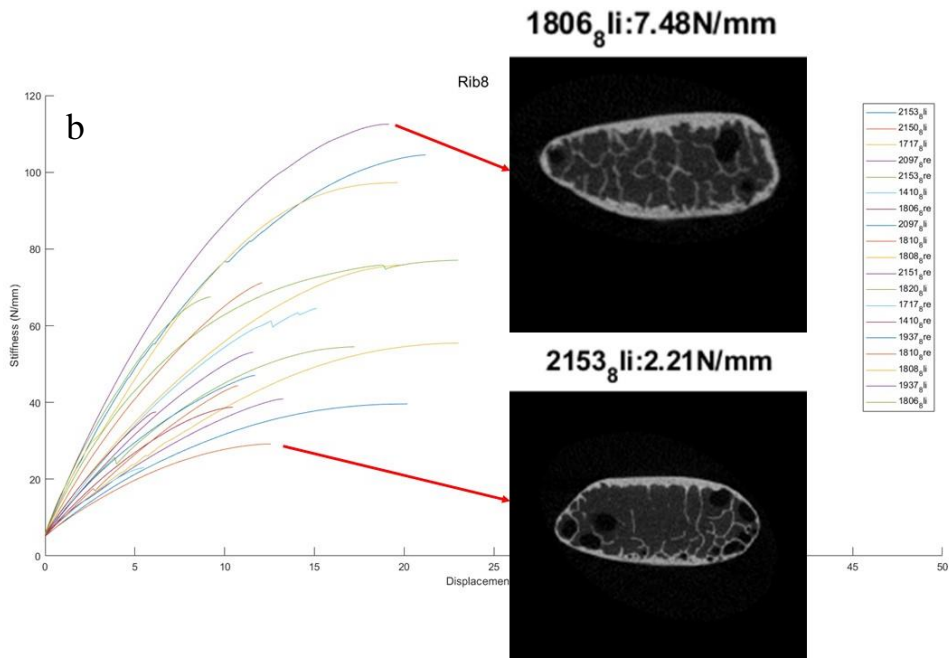
Figure 3.3-1: In (a) there are all the load displacement curves of fourth level rib; The two curves with the minimum and maximum break load values are correlated with their micro-CT scans. In (b) there are all the load displacement curves of eight rib level. The two curves with the minimum and the maximum stiffness values are correlated with their micro-CT scans.

The scans haven't equal dimensions: someone looks like zoomed. The inertia moments are considered in order to confirm the trends described above; however, it is not possible to appreciate any influences. The trabeculae values do not give any additional information.

Chapter 4 – Discussion

This Thesis aims to characterize the ribs analysing the global and local behaviour and exploring the microstructure. 89 ribs were tested in compression tests using a uniaxial testing machine. The local behaviour was explored using an optimized Digital Image Correlation approach. The bone microstructure close to the failure point was studied with micro-CT analysis.

The following discussion combines all the results in order to obtain a complete mechanical rib behaviour view.

4.1 Result analysis

From the global view, it seems that the break load, stiffness and energy assume higher values for lower level ribs. ANOVA not entirely confirmed this trend, but it could be possible to find an explanation considering the anatomical rib role. During breathing, the ribcage modifies its position and volume. This is possible thanks to the muscles involved which cause the ribs movement.

In particular, the lower ribs carry out larger movements. As a consequence, these ribs are subjected to physiological loads and deformations more frequently. Therefore a higher values of break loads and stiffnesses are mandatory for a proper breathing avoiding any failure risks.

Conversely, the upper ribs are not subjected to large movements as the inferior ones; they maintain the superior ribcage part in position. Thus the break load and the stiffness values are lower. The micro-CT scans validate these hypotheses showing a possible connection between the break load or the stiffness value with the rib structure.

Inside each group, an interesting trend is shown by the (load vs $\frac{Bone\ volume}{Tissue\ volume}$) and (stiffness vs $\frac{Bone\ volume}{Tissue\ volume}$) graphs. Generally the first one confirms that higher break load occurs if there is a certain bone quantity level. Contrarily, the relationship between (stiffness vs $\frac{Bone\ volume}{Tissue\ volume}$) shows that the Young modulus increase in ribs with lower bone tissue. It is important to observe that the $\frac{Bone\ volume}{Tissue\ volume}$ values belong only to break region.
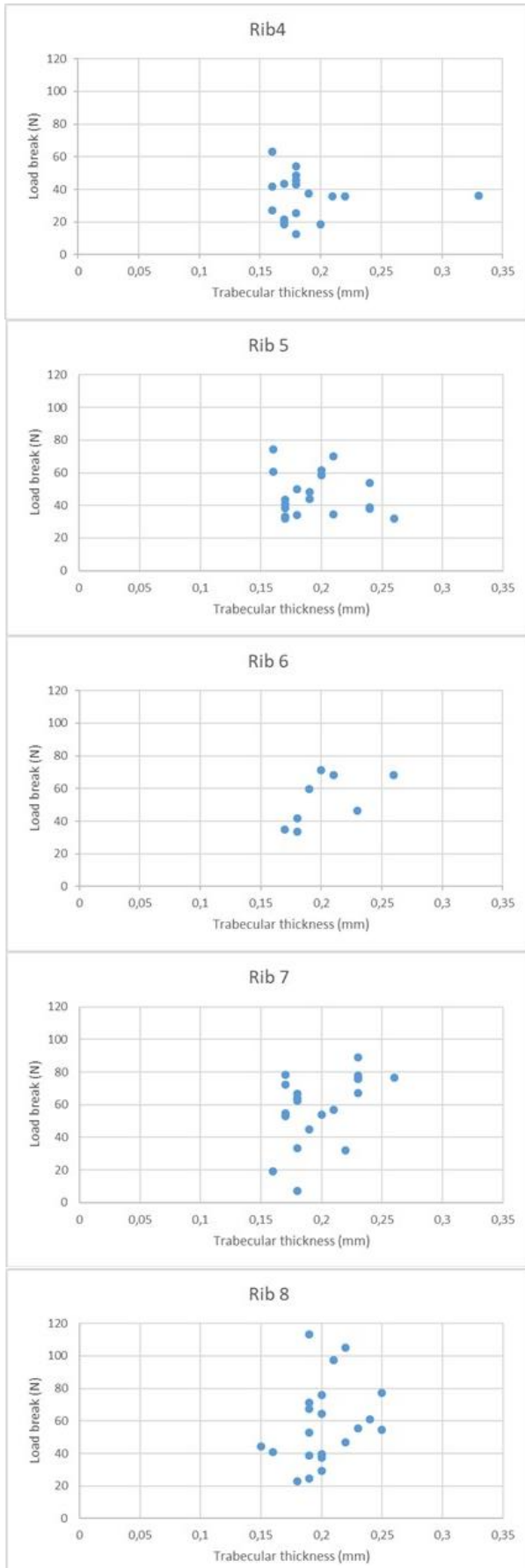
Figure 4.1-1: Break load vs trabecular thickness for each rib level.

It is important to observe that, despite these differences between ribs due to their positions, the energy absorbed for each rib group is quite similar according to ANOVA statistic. According to the biomechanic notions, the absorption capacity in bones is linked to the spongy bone presence. This is probably linked to the same trabecular organisation that all the ribs have in common; indeed it is possible to notice that the trabecular thicknesses values measured for each rib are quite similar between groups (Figure 4.1-1).

The strain visualisation represents the local analysis confirmation. Indeed higher strain values are measured in ribs with higher break load, according to the theory principles illustrated in the "Brief biomechanical notion" subchapter. In particular both the external and the internal side show in modulus higher $|\mathcal{E}_1|$ than $|\mathcal{E}_2|$. It is important to observe that, apart from $|\mathcal{E}_1|$ and $|\mathcal{E}_2|$ strain values, γ strains assume appreciable values in ribs. As a consequence, for each rib there is a ϑ angle between the reference system used and the one with the maximum strains. This indicates that for each rib was applied both flexion and torsion despite the machine was projected to apply only a bending moment. The graphs show that major angles can be

noticed for ribs which break loads belong from 40 to 60 N. Generally, the fifth, sixth and seventh ribs broke with this load values. A possible explanation could be linked to the rib's shape. According to the longitudinal rib view, the anterior and the posterior ends, are not perfectly aligned. Whereby the machine applies load in order to determine flexion on the specimen; to do that the anterior extremity movement determines shear strains on its surface because it is not aligned with the posterior one. The shear strains are due to torsion.

This phenomenon is confirmed looking at the maximum and minimum ε; their directions are slightly different from the longitudinal ones in some ribs; in addition, some specimen shows a particular strain direction that points up a torsion.
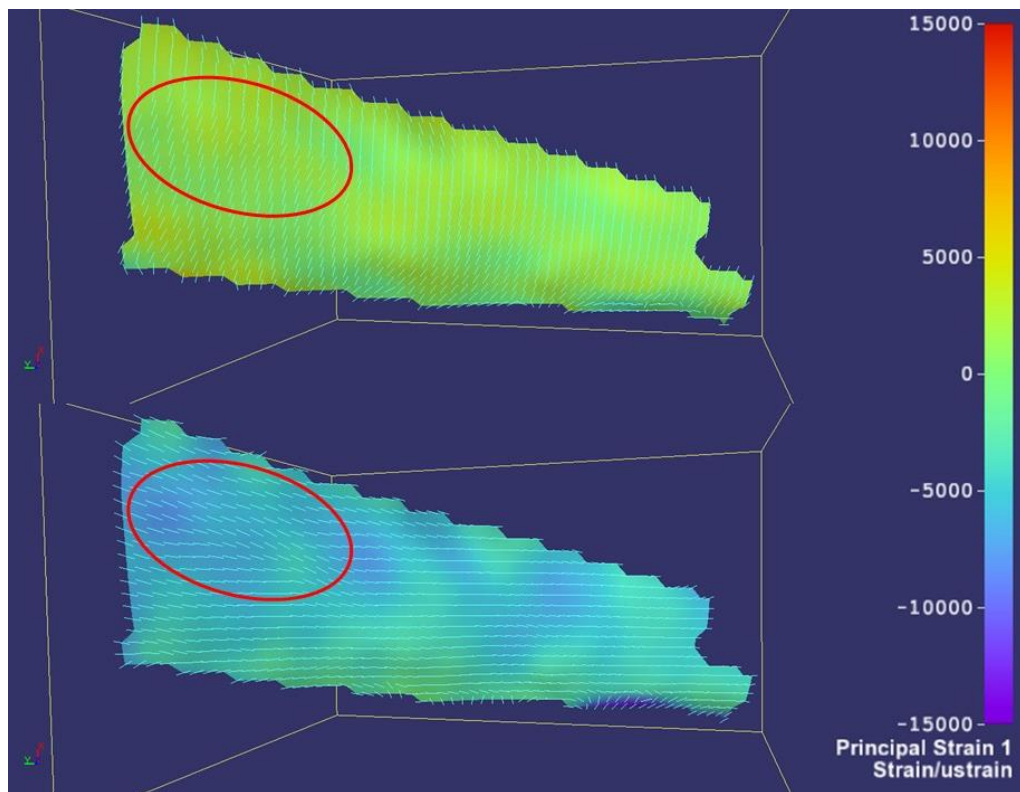

Figure 4.1-2: In this rib (1717_4r) it is possible to observe that the ε_1 and ε_2 in circles are inclined; maybe this phenomenon is due to torsion.

Unfortunately, it is not possible to determine a relationship between angles with the ε_1 and ε_2 directions measured for each rib.

With the data obtained, it is not possible to find why the ribs broke in fragile or "ductile" way. This is not linked to the presence of any cartilages, because every rib tested was constituted entirely by bone tissue. The reason could be explained through the buckling phenomena: it is a collapse that occurs at inferior load than the break one. This is confirmed by the means: indeed the "ductile fracture" measures a load value equal to 49,11 N whereas

the fragile ones 53,41 N. The buckling occurred for 31 ribs whereas the fragile occurred for 35 ribs (both horizontal and longitudinal fractures).

4.2 Limitation

Despite the methods, in this work some limitations occur.

- Monoaxial cell: this machine test could apply and measure only a load directed along a longitudinal direction. This means that the test machine could not estimate other new forces. However this configuration allows to execute all the tests in the same way.
- Constraints: the machine test does not show all the playing forces, because the tests are over constrained. This could be a possible representation of ribs embedded between the sternum and the corresponding vertebrae. However the test produce unknown forces. Probably the fractures are partly due to unmeasured load. For instance, the torsion assumes important unknown values useful for understanding the break reasons. Probably, isostatic tests could be useful to understand the failures only due to flexion. On the other hand, the DIC method could not be applied because the specimens could rotate during the tests: the DIC software probably could not correlate the images because the cameras would record different surfaces. Despite the possibility to record both sides, the internal one is less accurate because several times cameras were not able to record all the surfaces during the test. This means less accurate values and lack of information near the break point. However with this instrumentation is possible to study ribs from both sides.
- Load-displacement curves: as explained in the previous chapters, each rib is described by its load-displacement curve. The displacement is realized by the test machine, not by the specimens. Thus MATLAB script could produce less accurate images; despite that for each rib a general behaviour is provided. Extensimeter could produce more accurate results, but the preparation requires lot of time and the results are referred only to a partial surface. In addition there could be reinforcement effects.
- Mohr's circle: Another limitation is using the Mohr's circle for a surface: the calculus is implemented in surfaces near the point break. This is an abuse of this

theory because, Mohr's circle refers only to a point on the specimen, not to a surface. Despite that, it is a reasonable approximation.

Chapter 5 – Conclusion and future development

This Thesis faces up the rib mechanical behaviour studying them from three point of views:

- Global description: break loads, stiffnesses and energies are computed;
- Local description: the strains are visualised on the surface;
- Micro-CT scan: the rib microarchitecture is shown and the bone parameters are provided.

This analysis produced interesting results which can be used for deepening the rib mechanical properties. It seems that the characteristics are linked to the position in the ribcage: lower ribs show higher break loads and stiffnesses. The micro-CT scans confirmed that assumption showing the cortical and the trabecular bone which most influence the mechanical behaviour. The DIC method allows to calculate the strains on the specimen surface with a certain accuracy and precision. The strain analysis points out that ribs broke thanks to a combination of both flexion and torsion: this could be a reason to design another set-up, considering the DIC instrumentation.

The results obtained could be used for other studies about ribs. Indeed this Thesis describes only the starting evaluation of a complex work in which the University of Bologna and the University of Ulm are involved.

Bibliography

1. Liebsch C, Graf N, Wilke H-J. The effect of follower load on the intersegmental coupled motion characteristics of the human thoracic spine: An in vitro study using entire rib cage specimens. *Journal of Biomechanics*. 2018;78:36-44. doi:10.1016/j.jbiomech.2018.06.025

2. Holcombe SA, Kang Y-S, Derstine BA, Wang SC, Agnew AM. Regional maps of rib cortical bone thickness and cross-sectional geometry: Regional rib cortical thickness maps. *J Anat*. June 2019. doi:10.1111/joa.13045

3. Liebsch C, Graf N, Appelt K, Wilke H-J. The rib cage stabilizes the human thoracic spine: An in vitro study using stepwise reduction of rib cage structures. Garcia Aznar JM, ed. *PLoS ONE*. 2017;12(6):e0178733. doi:10.1371/journal.pone.0178733

4. Stawicki SP, Grossman MD, Hoey BA, Miller DL, Reed JF. Rib Fractures in the Elderly: A Marker of Injury Severity: RIB FRACTURES IN THE ELDERLY. *Journal of the American Geriatrics Society*. 2004;52(5):805-808. doi:10.1111/j.1532-5415.2004.52223.x

5. Anastasi G, Capitani,Silvano, Carnazza, Maria Luisa, et al. *Trattato Di Anatomia Umana*.

6. Beer F, Jhonson ER, DeWolf, Jhon T. *Mechanics of Materials*. Sixth edition. Milano: McGraw-Hill Education; 2014.

7. Pietrabissa R. *Biomateriali per Protesi e Organi Artificiali*. Bologna: Pàtron Editore; 2010.

8. Palanca M. Ottimizzazione dei parametri di acquisizione ed elaborazione per l'analisi di segmenti ossei tramite correlazione di immagini digitali. 2013.

9. Palanca M, Tozzi G, Cristofolini L. The use of digital image correlation in the biomechanical area: A review. *International Biomechanics*. 2016;3(1):1-21. doi:10.1080/23335432.2015.1117395

Thanks

È doveroso e necessario ringraziare tutti coloro che mi hanno accompagnato in questo percorso durato 3 anni. Perciò ho preferito scrivere questo piccolo paragrafo in Lingua Italiana, nella speranza di risultare più chiaro possibile.

L'elaborazione e l'approfondimento dell'argomento trattato sono stati possibili grazie al Professor Palanca, il quale, con pazienza e simpatia, mi ha permesso di intraprendere un interessante (seppur breve) percorso formativo durante questo secondo semestre, mostrandosi sempre disponibile in ogni occasione. Ringrazio il Relatore Professor Cristofolini che mi ha permesso di frequentare il laboratorio e ha sempre supervisionato il lavoro, indicando la strada migliore da percorrere. Ringrazio tutti i componenti del laboratorio di Biomeccanica che mi hanno aiutato durante l'elaborazione dei dati, mostrandosi sempre disponibili e volenterosi in ogni occasione.

Non posso dimenticarmi di ringraziare tutti i colleghi e le colleghe del corso con i quali ho fatto amicizia in questi tre anni; mi avete permesso di raggiungere questo obiettivo aiutandomi nei momenti di difficoltà e spronandomi a dare sempre il meglio. Spero vivamente di essere stato per voi una persona fedele e sincera.

Ringrazio i miei amici d'infanzia e liceo che, in vena scherzosa, sono stati sempre presenti nonostante le distanze; pur avendo stili di vita profondamente differenti, ho sempre trovato in voi un riferimento.

Ringrazio tutta la mia Famiglia che mi ha permesso di intraprendere questo percorso e di continuarlo in futuro, mostrandosi sempre pronta per ogni evenienza e difficoltà tramite consigli ed aneddoti di cui farò sempre tesoro.

Nonostante la semplicità, ho fatto molta fatica nel redigere questo ultimo paragrafo: avrei voluto esprimere tutta la mia gratitudine ma non sono stato in grado di vergarla su carta nel modo migliore. Spero che queste poche righe bastino per esprimere la mia riconoscenza verso tutti coloro che hanno rappresentato la mia bussola in questi tre anni.